Separation and Purification Technology 195 (2018) 413–430

Contents lists available at ScienceDirect

Separation and Purification Technology

journal homepage: www.elsevier.com/locate/seppur

Characterization of functionalized ionic liquids for a new quasi-isothermal chemical biogas upgrading process

Felix Ortloff[a,b,*], Markus Roschitz[a], Maria Ahrens[c], Frank Graf[a,b], Thomas Schubert[c], Thomas Kolb[a,b]

[a] DVGW Research Center at Engler-Bunte-Institute (DVGW-EBI), Karlsruhe Institute of Technology (KIT), Engler-Bunte-Ring 1, 76131 Karlsruhe, Germany
[b] Engler-Bunte-Institute, Fuel Technology Division (EBI ceb), Karlsruhe Institute of Technology (KIT), Engler-Bunte-Ring 1, 76131 Karlsruhe, Germany
[c] Ionic Liquids Technologies GmbH (IoLiTec), Salzstrasse 184, D-74076 Heilbronn, Germany

ARTICLE INFO

Keywords:
CO_2 separation
Chemical absorption
Ionic liquids
Biogas

ABSTRACT

In this work, a new CO_2 separation process using ionic liquid solvents is proposed. The approach focusses not only on improving the applied solvents or their CO_2 absorption chemistry, but also on adapting the separation process itself for exploiting the advantages of ionic liquids. This is achieved by adjusting the operating temperatures of the absorption and the regeneration columns of the upgrading process to the same moderate temperature level and operating the desorption of CO_2 under moderate vacuum instead of applying high grade heat from an external source.

In this article, the proposed CO_2 separation process is described in detail and the results of the development and characterization of appropriate ionic liquid solvents for applying the process to biogas upgrading are presented. The characterization section includes measurements on thermal and chemical stability, physical and chemical CO_2 solubility, physical CH_4 solubility, effective and intrinsic absorption kinetics, heat of reaction and various additional material properties of ionic liquid solvents. Physical gas solubility is examined for Room Temperature Ionic Liquids with [NTf_2], [Tf], [DCA] and [TCM] anions with imidazolium cations in a wide temperature range of 25–125 °C. The applied short chain [Tf] and [TCM] based RTIL feature a high selectivity concerning physical solubility of CO_2 and CH_4. Furthermore, the applied chemically functionalized IL (CFIL) show almost the double chemical CO_2 loading capacity than conventional amines. The measurements on absorption kinetics show that the absorption of CO_2 in the applied IL solvent in the desired temperature range is about as fast as when aqueous DEA is applied.

Based on the derived experimental results, an energetic evaluation of the process is carried out indicating that the proposed process enables considerable potentials for energetic savings, forming the basis for being close to economic feasibility within relatively short payback periods.

1. Introduction

Ionic liquids (IL) are molten salts consisting of rather large and asymmetric ions which sterically inhibit crystallization. Per definition, molten salts are referred to as “ionic liquids” in case they are liquid at temperatures below 100 °C. There even are some IL which are liquid at room temperature or below [1–3], namely RTIL (Room Temperature Ionic Liquids). Induced by their ionic nature IL feature a negligible vapor pressure p^*, even at elevated temperatures ($p^*(T < 150\,°C) < 10^{-5}$ Pa [4]). Therefore, applying ionic liquids for the removal of CO_2 from gas streams by absorption has been discussed in science ever since the class of substances gained public attention in early 21st century [2]. In the majority of examined cases in literature, CO_2 is to be removed from flue gas of coal fired power plants (post-combustion CCS), and IGCC units (pre-combustion CCS) [5], as CO_2 emissions from power production are in charge of the largest share of the world’s annual CO_2 emissions (35–40 $GtCO_2$ in 2015 [6]). Besides decarbonizing of flue gases, GHG emissions can also be reduced by substituting fossil fuels by renewables, e.g. by utilizing biomass based energy resources. Furthermore, the production and injection of substitute natural gas (SNG) from biomass offers several advantages compared to power production by e.g. wind and solar such as non-volatility, availability of the natural gas grid for distribution and storage purposes but also the possibility of utilizing the gas via alternative routes, e.g. in the transportation sector or as a sustainable carbon source for the chemical industry. SNG can be produced from biomass by either

* Corresponding author at: DVGW Research Center at Engler-Bunte-Institute (DVGW-EBI), Karlsruhe Institute of Technology (KIT), Engler-Bunte-Ring 1, 76131 Karlsruhe, Germany.
E-mail address: ortloff@dvgw-ebi.de (F. Ortloff).

https://doi.org/10.1016/j.seppur.2017.12.014
Received 17 August 2017; Received in revised form 4 December 2017; Accepted 4 December 2017
Available online 08 December 2017
1383-5866/

Nomenclature

A	surface area (m^2)
β	mass transfer coefficient (m/s)
B	loading capacity (mol/mol)
c	concentration (mol/m^3)
δ	thickness of diffusion limited boundary layer (m)
D	diffusion coefficient (m^2/s)
e	specific energy demand (kWh/m^3) (STP)
E	chemical enhancement factor (–)
E_A	activation energy (kJ/mol)
F	mass flow (kg/s)
η	dynamic viscosity (Pa s)
h	enthalpy (kJ/mol)
H	Henry coefficient (bar)
Ha	Hatta number (–)
i, j	indices (–)
k	reaction rate constant various
K	equilibrium constant (c^{-x})
N	number of species (mol)
m	mass (kg)
M	molar mass (g/mol)
ρ	density (kg/m^3)
p_i	(partial) pressure (of i) (bar)
r	reaction rate (various)
R	universal gas constant (8.314 kJ/(kmol·K))
σ	surface tension (N/m)
S	selectivity (–)
t	time (s)
T	temperature (°C or K)
V	volume (m^3)
x	molar fraction in liquid phase (–)
y	molar fraction in gas phase (–)
ω	mass fraction (–)

Abbreviations

cal	calculated
exp	experimental
g	gaseous state
IL	ionic liquid
l	liquid state
MPT	maximum process temperature
ppm	parts per million (on a molar base)
RTIL	room temperature ionic liquid
CFIL	chemically functionalized ionic liquid
STP	standard temperature and pressure

thermochemical conversion [7] in combination with syngas purification [8] and methanation [9] or by biochemical conversion plus subsequent gas upgrading [10,11]. Fig. 1 shows the corresponding biogas process chain.

Nowadays, the so called Power-to-gas (PtG) process [12] is an additional option for production of SNG from renewable electricity, with which the limited biomass potentials can largely be overcome.

In order to be allowed to inject the produced gas into the natural gas grid, country specific requirements for gas quality have to be met. In Germany these are in particular the technical guidelines G 260 [13], G 262 [14] of DVGW and for CNG vehicles the DIN 51624 [15]. Besides many other requirements on the gas quality, the methane content needs to be at minimum 95 mol%. As the CO_2 content of raw biogas (after fermentation) typically is 40–50 mol% [10,11], CO_2 removal is the major biogas upgrading task.

Compared to large-scale CO_2 removal from coal-fired power plants the requirements for CO_2 removal applied for biogas upgrading differ fundamentally:

- CO_2 is to be removed from a gas stream which mainly consists of methane not of N_2/O_2 (as in post-combustion CCS case) or of hydrogen (pre-combustion CCS) [16].
- Biogas plants are several orders of magnitude smaller than potential CCS plants in conventional power production scale. Thermal capacity of German biogas plants was 4.5 MW in average in 2014 [17], which means that ca. 350–500 m^3/h (STP) of CO_2 have to be removed from the biogas stream per plant. In conventional power production of flue gas streams on the order of 1–3 million m^3/h have to be treated [16]. Therefore, the total required solvent inventory is much smaller when the upgrading process is applied for biogas.
- Biogas plants are decentralized installations and often located in rural areas. Furthermore, adequate thermal integration of the biogas upgrading plant is not available, as on-site or nearby heat sources or heat sinks are often missing. Hence, biogas upgrading plants are typically driven by electric energy [10,11].

For the removal of CO_2 from biogas several upgrading technologies exist which differ by the applied gas separation technique and by the degree of process integration (Table 1).

Absorption [7] is a wide spread industrial process for sour gas treatment. Consequently, first plants for CO_2 removal from biogas were physical or chemical scrubbers, respectively. Both still feature the largest share in biogas upgrading in Germany [20], e.g. physical water or polyethyleneglycol-dimethylether (=Genosorb) scrubbing or chemical

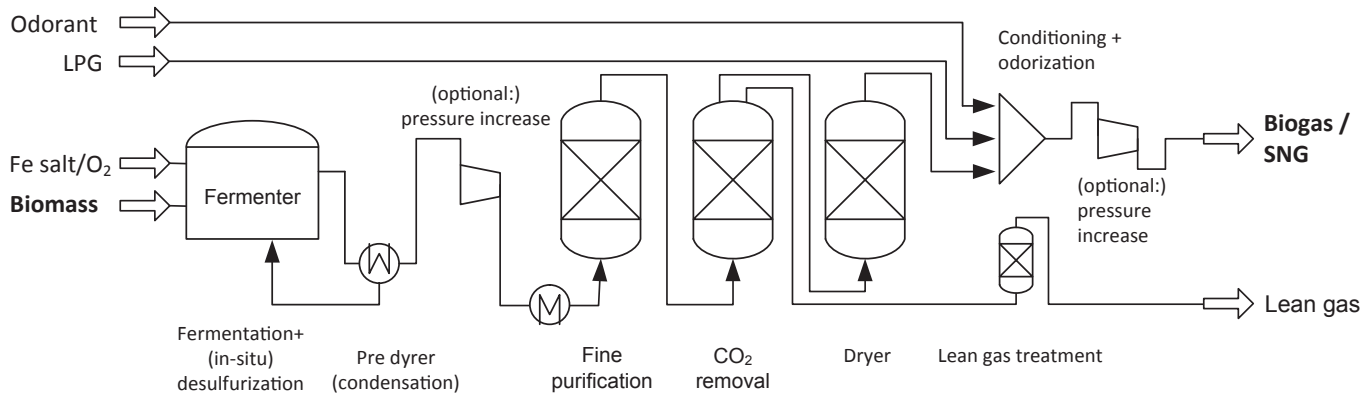

Fig. 1. Biogas production and upgrading for injection into the natural gas grid.

Table 1
State-of-the-art processes for CO_2-removal from biogas in Germany [10,11,18–20].

	Water scrubber	Genosorb® Scrubber	PSA	Chemical scrubber	Membrane separation
Market shares, Germany, 2015	31%	11%	22%	32%	4%
Operating principle	Absorption		Adsorption	Absorption + Reaction	Permeation
y_{CH_4} in Biomethane	< 99 vol%	< 98 vol%	< 98 vol%	> 99 vol%	< 98 vol%
y_{H_2S},max pre CO_2-removal	< 500 ppm	< 100 ppm	< 1–2 ppm		
Subsequent treatment necessary?	Drying, desulphurisation, CH_4-removal from lean gas	(drying), desulphurisation, CH_4-removal from lean gas	CH_4 removal from lean gas	Drying	(drying), CH_4 removal from lean gas
Operating pressure p	8 bar	8 bar	5 bar	1 bar	8–17 bar
Energy demand per raw biogas feed					
Electric energy demand e_{el} per raw biogas	0.23 kWh/m³	0.29 kWh/m³	0.25 kWh/m³	0.07 kWh/m³	0.2 kWh/m³
Thermal energy demand e_{th} per raw biogas	–	0.11 kWh/m³	–	0.60 kWh/m³	–

scrubbing by applying amines such as monoethanolamine (MEA), diethanolamine (DEA), methyldi-ethanolamine + piperazine (MDEA + PZ) or aqueous amino salt based solutions.

As shown in Table 1, biogas upgrading processes based on physical interactions with CO_2, such as physical scrubbing (see Fig. 2), but also PSA and membrane separation, suffer from a rather high electric energy demand due to the necessity of feed gas compression (C-01 and C-02) and due to internal recompression efforts for reduction of methane loss.

However, chemical absorption (Fig. 3), which is typically operated at ambient pressure, requires a large amount of thermal energy for regeneration of the solvent, namely to introduce the heat of reaction of e.g. the deprotonation of protonated amines (e.g. $MEAH^+$) [21] at a temperature level of typically 120–160 °C.

Instead of applying the common optimization strategy for chemical scrubbing processes, which is to develop new solvents or solvent blends featuring a reduction of heat of reaction during CO_2 uptake, this work focuses on a different approach. Within the proposed gas upgrading concept the operating temperatures of the absorption and regeneration devices (Col-01–Col-03 in Fig. 4) are adjusted to approximately the same temperature level of about 80 °C. As the temperature remains almost constant in the entire process, the change in operating concept is associated with the benefit that the thermal energy for regeneration of the solvent does not have to be supplied from an external source.

Except of obvious thermal losses to the ambient, which cannot be avoided entirely when such a process is operated at an increased temperature level, the solvent does not have to be heated nor cooled while circulating between the columns. But, as a chemical driving force for regeneration of the solvent is mandatory, the regeneration of the solvent is carried out by a reduction of pressure in the regeneration units instead (C-01 and C-02).

Such type of operating concept cannot be implemented using conventional solvents as they typically exhibit a high vapor pressure (as they are aqueous mixtures). Therefore large parts of the thermal energy of the system would be dissipated by evaporating the solvent or water, respectively. Hence, the upgrading concept as proposed in Fig. 4 requires a new type of solvent with a negligible vapor pressure, which leads to ionic liquids.

With the applied concept the major drawback of ionic liquids, their increased viscosity compared to common aqueous solutions, leading to mass transfer limitations, can be partly overcome by the higher operating temperature of the entire process. Certainly an increase of absorption temperature also leads to a reduction of solvent utilization efficiency (by means of actual CO_2 uptake per maximum theoretical CO_2 uptake of the solvent per cycle), but as the temperature of the solvent stream does not have to be increased for regeneration, a high solvent utilization efficiency is not crucial - especially not as the energy demand for solvent circulation is typically low when chemical scrubbing is applied and the pressure differences between the columns are low.

For implementing such a process it was necessary to identify

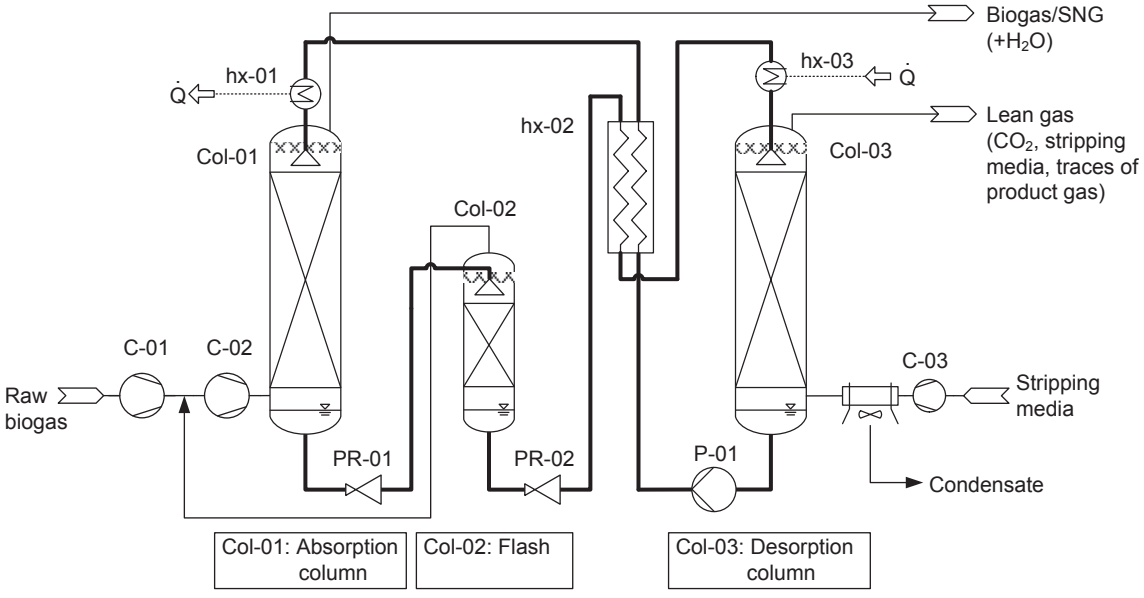

Fig. 2. Flow sheet of biogas upgrading by physical absorption.

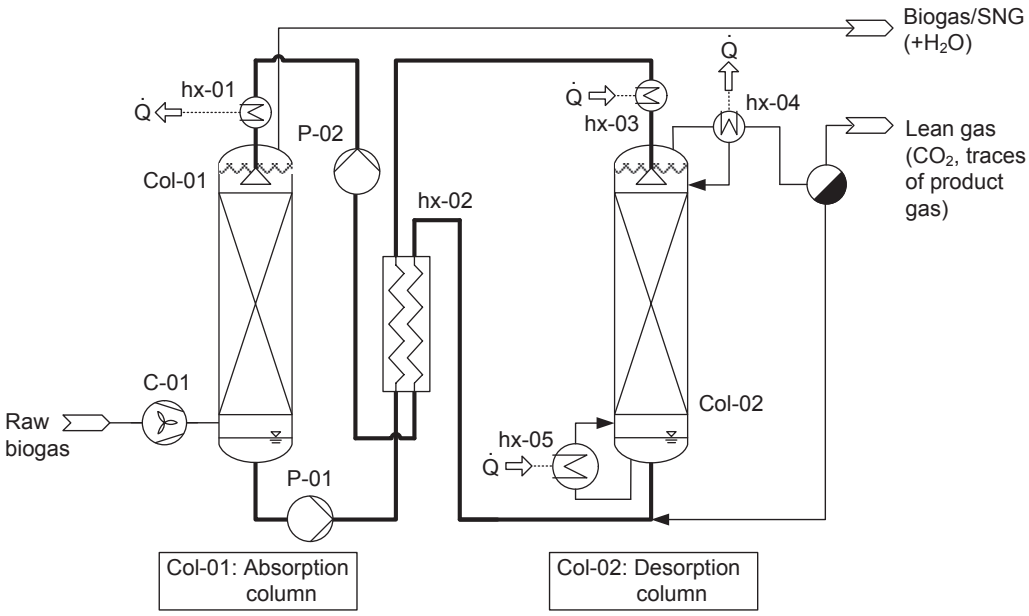

Fig. 3. Flow sheet of biogas upgrading by chemical absorption.

suitable ionic liquid solvents for the proposed upgrading concept. Section 2 of this work gives an overview of the tested RTIL and CFIL. Section 3 shows the results of characterization of the most important solvent properties, such as thermal and chemical stability, CO_2 uptake, reaction kinetics and heat of absorption (for chemical reaction with CO_2). Vapor pressure is not further examined in this work, detailed information can be taken from Heym et al. [4].

Finally, based on the experimental results, a first estimation of energetic efficiency of the process is given in Section 4 and the results are compared with state-of-the-art technologies for CO_2 removal from biogas.

2. Applied materials and IL synthesis

For the proposed process a new ionic liquid based solvent was developed. Right from the beginning the solvent has been chosen to be a mixture of RTIL and CFIL as pure CFIL suffer far too high viscosities to be applied to conventional mass transfer equipment [5] alone. In many cases viscosity even rises during CO_2 uptake due to an increase of charge density and H bonds in the ionic liquid [5]. The main task of the RTIL in the solvent mixture therefore is to reduce the viscosity of the solvent mixture.

The examined CFIL were restricted to anion functionalization. In majority deprotonated amino acids were applied as there are relatively cheap. The major task of the CFIL is to provide competitive absorption kinetics, high selectivity and a suitable CO_2 absorption isotherm, characterized by an appropriate CO_2 loading capacity but even more important, a rather moderate capacity gradient at low partial pressures of CO_2. This is mandatory as the solvent temperature is to be kept constant within the upgrading process and CO_2 is to be stripped out of

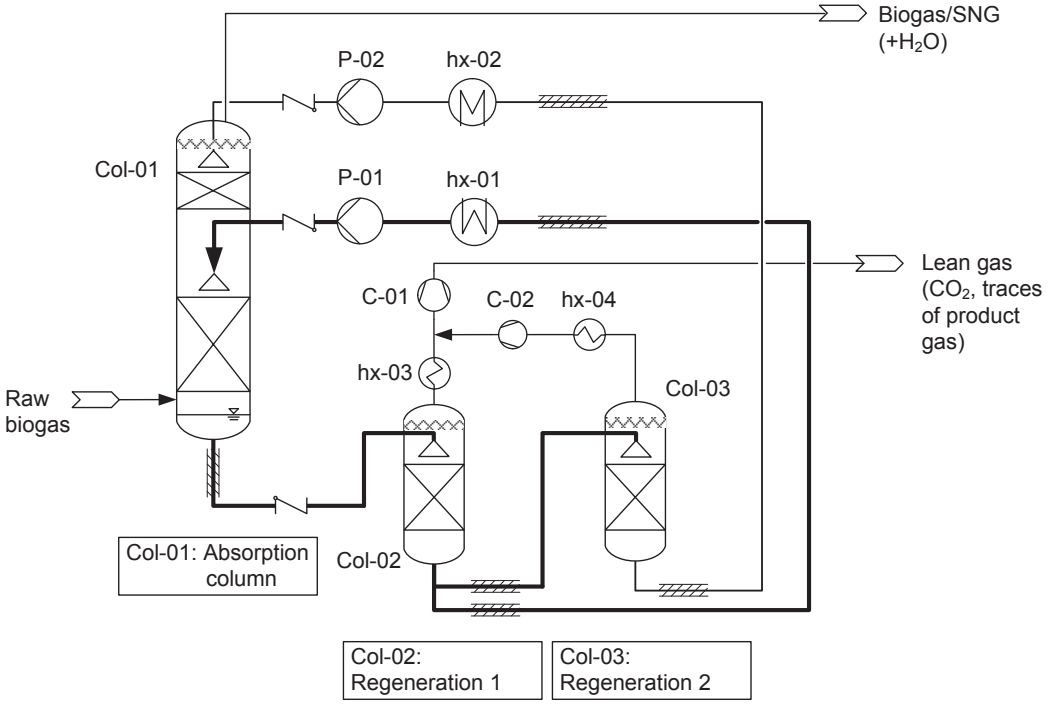

Fig. 4. Process concept for nearly isothermal chemical scrubbing with ionic liquid solvents.

the solvent by pressure reduction.

Concerning RTIL, imidazolium cations with sulfate (R-SO_4), tetrafluoroborate (BF_4), hexafluorophosphate (PF_6), sulfonates (R-SO_3), dicyanamide (DCA), tricyanomethanide (TCM), trifluoromethanesulfonate (Tf) and bis(trifluoromethylsulfonyl)imide (NTf_2) anions are most common. Halogenide anions are often too small to form a RTIL. BF_4 and PF_6 decompose in presence of water at increased temperatures (resulting in formation of HF). Alkylsulfates tend to hydrolyze under formation of HSO_4, sulfonates suffer a relatively high viscosity. Reasonable options of RTIL for the desired application therefore are DCA, TCM, NTf_2 and short chain Tf anions. While NTf_2 and Tf anions are known to be quite stable from the chemical and thermal perspective, DCA and TCM anions do not consist of any halogens, which make them the better choice from the environmental perspective.

Concerning many available CFIL, the reaction mechanism with CO_2 is often still under discussion, especially when higher temperatures are considered. In order to be able to compare with conventional amines, corresponding amine functionalized CFIL anions were chosen (see Table 2). Similar to conventional amine solvents, CFIL with primary (alaninate [Ala]), secondary (prolinate [Pro]) and tertiary anions (dimethylglycinate [Gly] + PZ) were applied. For further examination of the role of the acidic H in 2-Position of the imidazolium ring, an alkylated cation, namely [BDiMIM], was selected and compared with the results of a [BMIM] based IL.

2.1. Preparation of the applied CFIL

Depending on the availability of precursors, the amine functionalized ionic liquids were prepared starting from the bromide or the chloride salts of the corresponding cations, then transferred into the hydroxide form via anion exchange resin (Cl-type, pretreated by 5 M NaOH solution) and neutralized by drop-wise addition into the particular amino acid, which was supplied in 1.02 fold excess in aqueous solution [22–24]. The reaction was carried out at room temperature for at least 12 h. After appropriate post-treatment the resulting substances were dried under vacuum at 60 °C for at least 36 h. Acetonitrile was added to accelerate the water removal. The alaninate ([Ala]) based CFIL received is a light yellow solid, [BDiMIM][Pro] a yellow jellylike solid. [BMIM][Pro] and [BDiMIM][Gly] are liquid at room temperature but show a more intense yellow color. The product quality and the residual halide content of the synthesized IL were checked by using ^{1}H-, ^{13}C NMR (Avance AV400 by Brucker) and IC (ICS-90 by Dionex), respectively. The water content of the ionic liquids was obtained via Karl-Fisher titration (AQUA 40.00 by Analytic Jena). Detailed information on the applied chemicals is supplied in Table 3. In any of the applied ionic liquids or IL mixtures, halides were below 200 ppm and the residual water content was lower than 150 ppm.

3. Characterization and evaluation of IL solvents

The characterization section of this work focusses on the physical properties for application of the examined solvents in the CO_2 scrubbing process by near-isothermal absorption. Thermal and chemical stability (Section 3.1), CO_2 uptake (Section 3.2) and reaction kinetics (Section 3.3) are of special interest within this study. Besides, some additional standard material properties of the applied substances are given.

Literature overview

Various data on absorption of CO_2 in ionic liquids in both, RTIL and CFIL is available in literature [5]. As high solvent utilization efficiencies are of special interest in conventional operating mode of CO_2 scrubbing systems, CO_2 absorption data at near ambient temperature is most common. Data on high temperature absorption for RTIL and for CFIL is rare.

It is known from conventional gas upgrading processes that the regeneration of amine based solvents for CO_2 capture requires at least temperatures of around 60–80 °C. This vice versa marks the minimum operation temperature of the proposed isothermal upgrading process. Gas solubility data of CO_2 and CH_4 in IL is available only for $T < 70$ °C, in the majority of cases for even lower temperature, e.g. in the range between 5 and 40 °C. However, density and viscosity data is available for higher temperatures up to approximately 120 °C but not for all RTIL of interest. Table 4 gives an overview of available data on RTIL in literature.

3.1. Thermal and chemical stability

Even though many data on thermal stability of IL is available, it is known from own experience that there are significant overestimations present in literature values, especially when long term stability is considered. Therefore, TGA experiments for determination of thermal and chemical stability were carried out with all IL shown in Table 4 in a temperature range from 348.13 to 473.13 K in a Netzsch TG 209 F1 Iris thermogravimetric analyzer (TGA). The mass loss of the samples was tracked in isothermal segments at the desired temperatures for at least 8 h. For each measurement samples of approximately 20 mg were applied to an alumina crucible and placed into the TGA. In advance of any measurement the setup was evacuated and purged with nitrogen for at least three times in order to remove any other gases from the measurement chamber. Thereafter, heating was applied to the sample with a heating rate of 10 K/min under nitrogen atmosphere. Once heated up, the gas atmosphere of interest was applied. For thermal stability measurements nitrogen was applied, for measurement of chemical stability oxygen was added in various ratios.

Thermal stability of RTIL

As shown in Fig. 5, RTIL with [NTf_2] and [Tf] anions are stable at 473.15 K. This finding corresponds with literature findings, where thermal stability of this type of IL is typically specified in the range of

Table 2
Common amines for CO_2 absorption and corresponding chemically functionalized ionic liquids (CFIL) with amine functionalization of the ILs' anions.

Common amines	e.g.	Characteristics	Reaction equation	IL
Primary	MEA	reaction kinetics ↑ heat of reaction ↑ CO_2 capacity ↓ thermal stability ↓	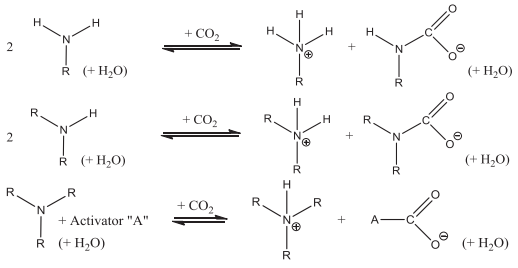	[K^+][Ala]
Secondary	DEA			[K^+][Pro]
Tertiary	MDEA			[K^+][Gly] + PZ

Table 3
Applied chemicals.

Abbreviation	Chemical formula	Molecular formula	Molar weight M	Chemical structure	CAS-No.	Supplier
MEA	Monoethanolamine	C_2H_7NO	61.08	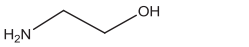	141-43-5	Merck
DEA	Diethanolamine	$C_4H_{11}NO_2$	105.14	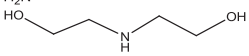	111-42-2	Merck
MDEA	Methyl-diethanolamine	$C_5H_{13}NO_2$	199.16	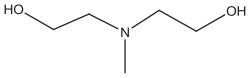	105-59-9	Merck
PZ	Piperazine	$C_4H_{10}N_2$	86.14	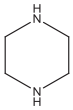	110-85-0	Merck
DL-Alanine	DL-Alanine	$C_3H_7NO_2$	89.10	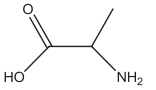	302-72-7	Merck
DL-Proline	DL-Proline	$C_5H_9NO_2$	115.13	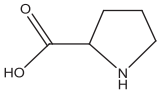	609-36-9	Merck
Dimethyl-glycine	Dimethyl-glycine	$C_4H_9NO_2$	103.12	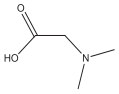	1118-68-9	Merck
[BDiMIM]Cl^-	1-Butyl-2,3-dimethylimidazolium chloride	$C_9H_{17}ClN_2$	188.7	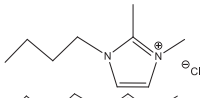	98892-75-2	IoLiTec
[BMIM]Cl^-	1-Butyl-3-methylimidazolium chloride	$C_8H_{15}ClN_2$	174.68	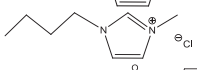	79917-90-1	IoLiTec
[EMIM][Pro]	1-Ethyl-3-methylimidazolium prolinate	$C_{11}H_{19}N_3O_2$	225.29	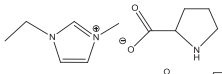	–	IoLiTec
[BMIM][Pro]	1-Butyl-3-methylimidazolium prolinate	$C_{13}H_{23}N_3O_2$	253.34	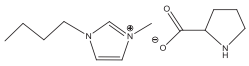	–	IoLiTec
[BDiMIM][Ala]	1-Butyl-2,3-dimethylimidazolium alalinate	$C_{12}H_{23}N_3O_2$	241.33	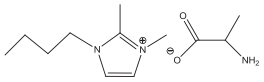	–	Own synthesis
[BDiMIM][Pro]	1-Butyl-2,3-dimethylimidazolium prolinate	$C_{14}H_{25}N_3O_2$	267.37	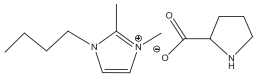	–	Own synthesis/ IoLiTec
[BDiMIM][Gly]	1-Butyl-2,3-dimethylimidazolium gylcinate	$C_{13}H_{25}N_3O_2$	255.36	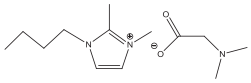	–	Own synthesis
[BDiMIM][NTf_2]	1-Butyl-2,3-dimethylimidazolium bis (trifluorosulfonyl)imide	$C_{11}H_{17}F_6N_3O_4S_2$	433.39	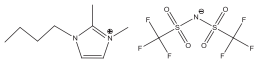	350493-08-2	IoLiTec
[BMIM][NTf_2]	1-Butyl-3-methylimidazolium bis (trifluorosulfonyl)imide	$C_{10}H_{15}F_6N_3O_4S_2$	419.36	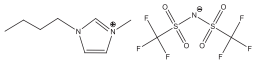	174899-83-3	IoLiTec
[EMIM][TCM]	1-Ethyl-3-methylimidazolium tricyanomethanide	$C_{10}H_{11}N_5$	201.23	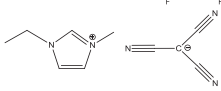	–	IoLiTec
[BDiMIM][TCM]	1-Butyl-2,3-dimethylimidazolium tricyanomethanide	$C_{13}H_{17}N_5$	243.28	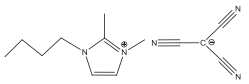	–	IoLiTec
[BMIM][TCM]	1-Butyl-3-methylimidazolium tricyanomethanide	$C_{12}H_{15}N_5$	229.28	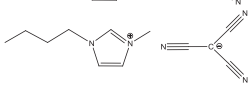	–	IoLiTec
[BMIM][DCA]	1-Butyl-3-methylimidazolium dicyanamide	$C_{10}H_{15}N_5$	205.26	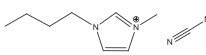	448245-52-1	IoLiTec
[BMIM][Tf]	1-Butyl-3-methylimidazolium trifluoromethanesulfonate	$C_9H_{15}F_3N_2O_3S$	288.29	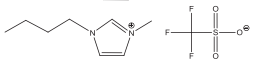	174899-66-2	IoLiTec

473.2–573.2 °C [4].

T = 473.15 KRTIL with [DCA] or [TCM] anions are less stable. Fig. 6 shows results of [BMIM][DCA] measurements in the temperature range from 398.15 to 473.15 K. Below 398.15 K no mass loss is detected. At 423.15 K approximately 1 wt% of the sample was lost due to evaporation of the decomposition products during the measurement period.

The lower thermal stability of ionic liquids with [DCA] and [TCM] anions in comparison to those with [NTf_2] and [Tf] anions is due to the higher basicity and nucleophilicity. Vaghjiani et al. [47] proposed the

Table 4
Overview of available literature data of RTIL of interest.

IL	T_{max}/K	Lit./–	ρ_{IL}/(kg/m^3)	T_ρ/K	Lit./–	η_{IL}/mPa s	T_η/K	Lit./–	H_{CO_2}/bar	T_{HCO_2}/K	Lit./–	H_{CH_4}/bar	T_{HCH_4}/K	Lit./–
[EMIM][DCA]	393.2	[25]	1105	293–353	[26]	17.5	293–353	[26]	78	303	[27]	2000	313	[28]
[EMIM][TCM]	433.2	[25]	1082	297	[*]	14.2	298	[*]	60	308	[**]	1050	298	[**]
[EMIM][Tf]	523	[29]	1384	278–348	[30]	40.7	278–348	[30]	57	278–338	[*]	1560	278–338	[*]
[EMIM][NTf_2]	523	[31]	1518	293–391	[32]	29	293–391	[32]	38.6	283–343	[33]	587.5	298–343	[34]
[BMIM][DCA]	473.2	[35]	1061	293–363	[36]	24.4	293–363	[37]	60.3	n/a	[38]	1273	298	[*]
[BMIM][TCM]	473.2	[39]	943	298	[40]	25.7	298	[*]	44	309	[41]	900	298	[**]
[BMIM][Tf]	6822	[42]	1290	295	[*]	70.4	283–343	[43]	42	303–342	[44]	n/a	n/a	n/a
[BMIM][NTf_2]	712.3	[31]	1438	293–391	[32]	51	273–353	[45]	34.3	283–323	[46]	467	298	[*]

* Own measurements.
** Kroon, M. et al. CCS Conference, 28.-29.05.2013, Antwerpen.

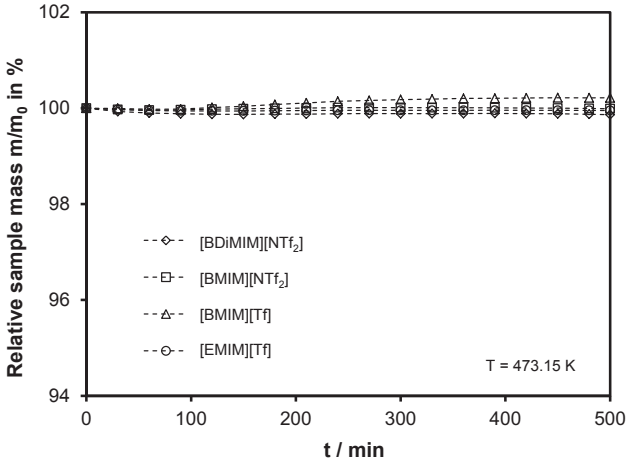

Fig. 5. TGA data RTIL with [NTf_2] and [Tf] anions at 473.15 K.

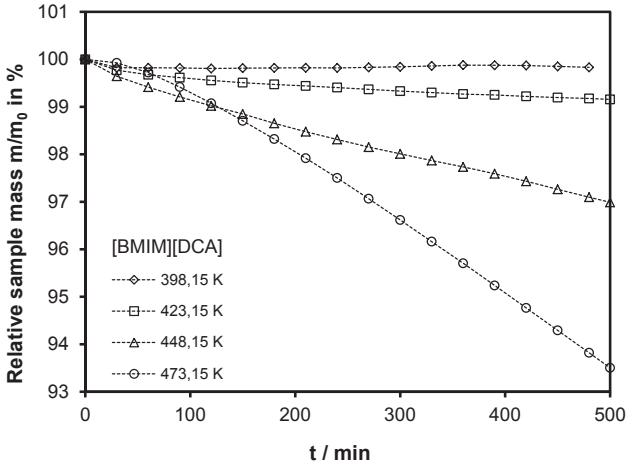

Fig. 6. TGA data of [BMIM][DCA] in a temperature range of 398.15–473.15 K.

thermal decomposition of ionic liquids with [DCA] and [TCM] anions under

(a) deprotonation of the C2-position on the imidazolium ring by the anion and
(b) S_N2-type reaction of the anion with the alkyl-substituents on the imidazolium ring (Fig. 7).

In addition, polymerization of the [DCA] and [TCM] anion is observed at higher temperatures. Nevertheless, 398.15 K is sufficient to be applied to the proposed upgrading process.

Thermal stability of CFIL:

CFIL are not as stable as RTIL at high temperatures as the amine groups tend to deprotonate. With CFIL, decomposition of the anion accounts for the decomposition of the ionic liquid [48]. The CFIL anions degrade under formation of carbon dioxide, carbon monoxide and ammonia [49]. The decomposition mechanisms are not yet understood. Fig. 8 shows TGA results for [BDIMIM][Pro]. At 348.15 K and 373.15 K [BDIMIM][Pro] seems to be stable. Above 373.15 K a decomposition of the CFIL within the measurement period becomes visible. At 423.15 K > 20 wt% of the CFIL is decomposed after 500 min.

Evaluation of maximum admissible process temperature (MPT)

Even though the individual TGA measurements were operated for at least 8 h, this is still a very short period when it comes to determining long-term stability. Technical processes are typically operated > 8000 h per year. If the IL based solvents shall be applied for CO_2 separation, information on long-term maximum operating temperature is needed. Therefore, based on the derived experimental TGA data, the maximum admissible process temperatures (MPT) were calculated by assuming a first order decomposition reaction of the IL (as proposed in literature [50]) and evaluating the individual kinetic decomposition parameters k_0 and E_A for each IL (Eq. (1)).

$$-r_i(T) = -\frac{dm}{dt} = k_{0,i}\exp\left(\frac{E_{A,i}}{RT}\right)m(t) \quad (1)$$

The decomposition rate r_i was calculated from the measured data at various temperatures and plotted in an Arrhenius type of diagram (see Fig. 9). The activation energies $E_{A,i}$ of the decomposition reaction and the kinetic parameters $k_{0,i}$ of the examined IL were be calculated from the slope of the curves and from the ordinate intercept, respectively. For determining the MPTs, a mass loss of 10 wt% of IL per year (8000 h TOS) was specified as acceptable. The corresponding maximum admissible process temperatures are given in Table 5.

Chemical stability of CFIL

Typically amines are sensitive to degradation when contacted with oxygen at elevated temperatures [16]. As there are always at least some traces of oxygen present in biogas, the influence of oxygen on the stability of the applied CFIL was examined. In general, the same methodology as for determining the thermal stability was applied but 375 ppmv, 5 vol% and 15 vol% of oxygen was added to the feed gas mixture. Fig. 9 shows the corresponding TGA results for [BDiMIM][Pro], as

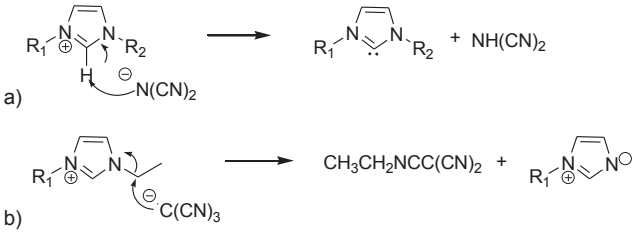

Fig. 7. Possible decomposition pathways (a) deprotonation of the C2-Position, (b) S_N2-type reaction of the anion with the alykl-substitutent.

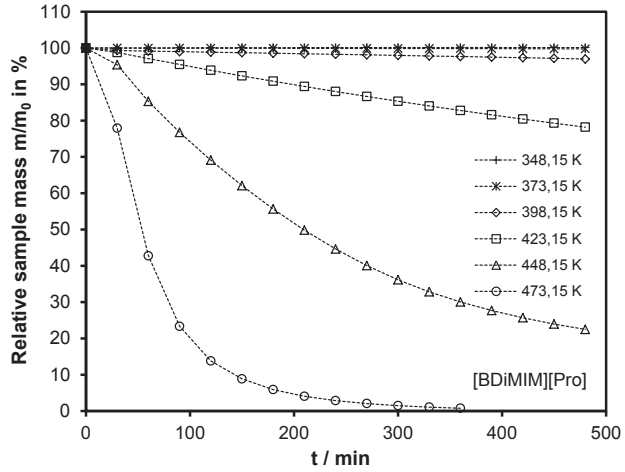

Fig. 8. TGA data of [BDIMIM][Pro] in a temperature range of 348.15–473.15 K.

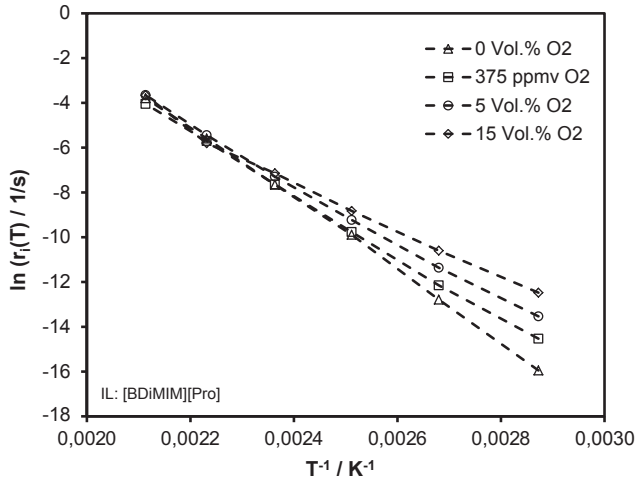

Fig. 9. Degradation rates of [BDiMIM][Pro] under various concentrations of oxygen.

Table 5
Maximum admissible process temperatures (MPT) of the applied RTIL.

Cation	Anion	E_A/kJ·mol^{-1}	ln(k_0)	MPT/K
RTIL				
[BDiMIM]	[NTf_2]	–	–	> 473.2
[BMIM]	[DCA]	159.9	32.4	402.6
	[Tf]	–	–	> 473.2
	[TCM]	106.5	15.8	410.5
	[NTf_2]	–	–	> 473.2
[EMIM]	[DCA]	159.2	32.7	398.4
	[Tf]	–	–	> 473.2
	[TCM]	101.4	14.8	403.7
	[NTf_2]	–	–	> 473.2

[BDiMIM][Pro] showed the highest thermal stability of the examined CFIL. As expected, oxygen enhances CFIL degradation. Adding 375 ppmv of oxygen already shows a slight effect, 5 vol% of oxygen increases the degradation rate considerably. Consequently, similar to conventional amines, a removal of oxygen prior to the IL based scrubbing unit is recommended in order to improve the durability of the upgrading process, e.g. by utilizing (bio-)methane for reduction of oxygen [51,52]. Table 7 includes the MPT values of [BDiMIM][Pro] under addition of oxygen.

Table 6
Maximum admissible process temperatures (MPT) of the applied CFIL.

CFIL				
CFIL	y_{O2}	E_A/kJ·mol^{-1}	ln(k_0)	MPT/K
[BDiMIM]	[Ala]	113.7	24.2	345.3
	[Pro]	133.3	30.2	351.7
	[N,N-DiMGly]	92.7	19.0	324.2
[BMIM]	[Pro]	102.4	22.0	329.2
[PMIM]	[Ac]	95.1	19.9	324.2

Table 7
Maximum admissible process temperatures (MPT) of the applied CFIL with oxygen.

CFIL + Oxygen				
CFIL	y_{O2}	E_A/kJ·mol^{-1}	ln(k_0)	MPT/K
[BDiMIM][Pro]	0%	133.3	30.2	351.7
	375 ppm	119.3	26.3	344.3
	5%	106.4	24.9	336.8
	15%	96.7	20.6	321.4

Conclusions on thermal and chemical stability of RTIL and CFIL

As summarized in Table 5, any of the tested RTIL shows sufficient thermal stability to be applied to the proposed process for long term at temperatures of up to 398.15 K (125 °C).

Concerning the stability of the CFIL, the application of BDiMIM cation leads to an increase of thermal stability of 20 K in comparison to the corresponding [BMIM] cation (see Table 6) due to alkylation of the acidic C2 position of the imidazolium ring.

The secondary prolinate based CFIL shows a higher stability as the primary alaninate anion. Against common expectations the tertiary dimethylglycinate anion has a reduced thermal stability as compared to the prolinate anion, which might be a consequence of the cyclic structure of the prolinate. The [BDiMIM][Pro] IL is thermally stable at temperatures of up to approximately 80 °C, which is sufficient for the desired process, but very close to the limit.

In future, further efforts should be undertaken to evaluate the decomposition mechanism of the CFIL in detail and consequently improve the thermal stability of the CFIL by altering the chemical structure based on these findings.

As mentioned, oxygen accelerates the decomposition of CFIL and leads to a lower MPT (see Fig. 9). An oxygen concentration of only 375 ppmv already causes a reduction of about 7 K in the maximum admissible process temperature (Table 7). Pre-treatment of the raw biogas before entering the CO_2 separation is advisable for a long lifetime of the solvent.

3.2. Physical and chemical CO_2 absorption capacities

The solubility of CO_2 and CH_4 are important parameters for the design of absorption processes as they define the amount of liquid needed per cycle for removal of CO_2 from the gas stream, but also enable the calculation of methane loss by co-absorption in the liquid. Therefore, both physical and chemical CO_2 absorption capacities were measured for the IL of interest.

Experimental setup

The solubility of carbon dioxide and methane was determined with the experimental setup shown in Fig. 10(l). The applied system consists of an agitated glass autoclave tempered by thermal oil and an additional reference gas cylinder, both with defined volumes. The autoclave (mini clave steel by Büchi Glas Uster AG) has a volume of ca. 150 mL and can be pressurized up to 10 bar and heated to 240 °C. The reference gas cylinder is applied for determination of the amount of gas charged

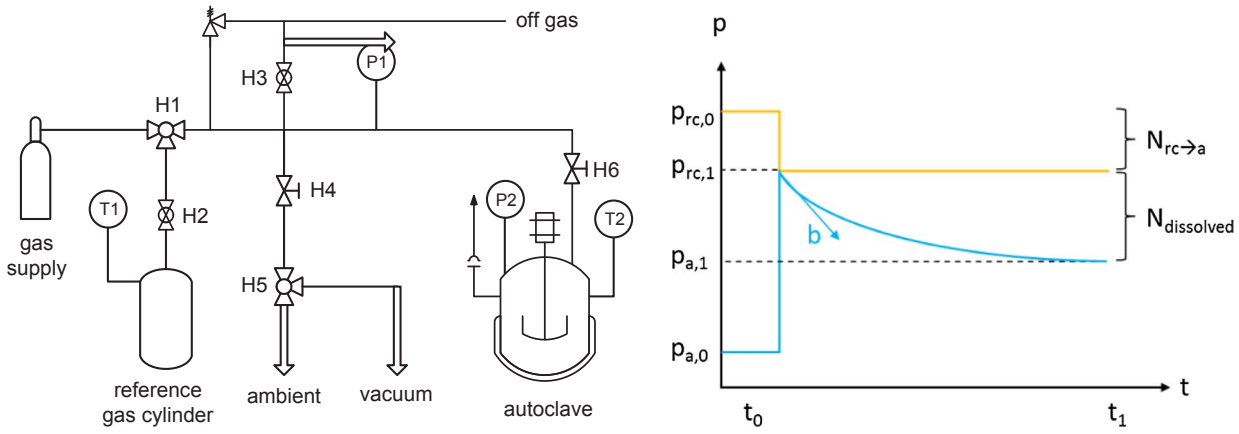

Fig. 10. Experimental setup for determination of gas solubility and absorption kinetics (l), and schematic pressure profile of a measurement (r).

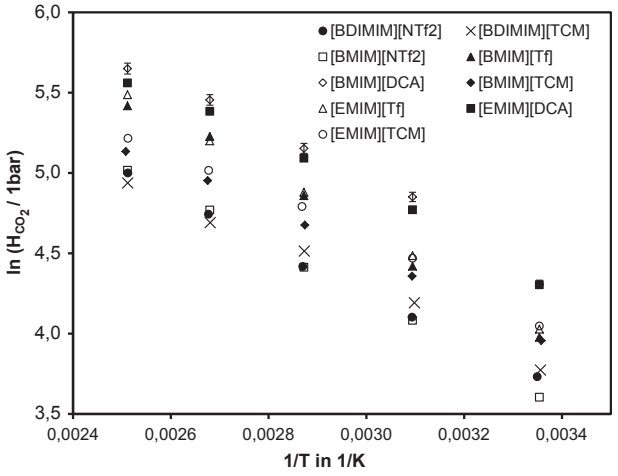

Fig. 11. Low pressure CO_2 solubility in [BDiMIM], [BMIM] and [EMIM] IL with [NTf_2], [TCM], [Tf] and [DCA] anions in the temperature range of 25–125 °C.

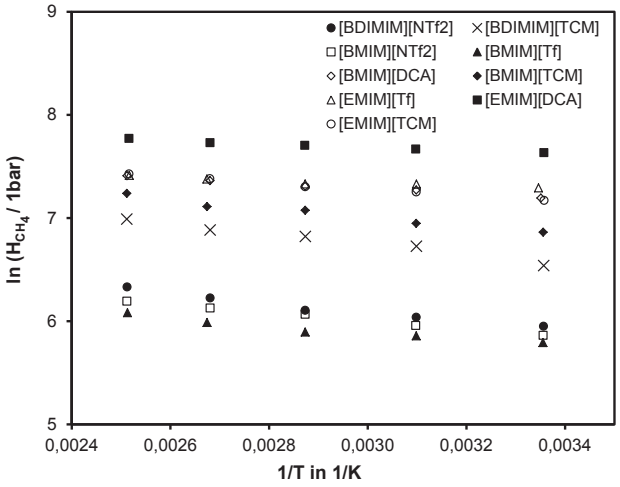

Fig. 12. Low pressure CH_4 solubility in [BDiMIM], [BMIM] and [EMIM] IL with [NTf_2], [TCM], [Tf] and [DCA] anions in the temperature range of 25–125 °C.

into the autoclave. The system pressure is monitored with two high precision pressure transducers, Type D-10, supplied by WIKA SE & Co. KG, providing an accuracy of 0.05% F.S. Gas (CO_2: 5.5; CH_4: 3.5) is supplied by Air Liquide in standard gas cylinders connected to the apparatus.

In advance of each solubility experiment the RTIL were stripped by applying vacuum at T = 100 °C for at least one hour in order to remove traces of water and/or other impurities. For measuring the gas solubility, a defined volume of liquid sample V_L is mixed with a known amount of gas at a given pressure $p_{rc,1}$ in the autoclave. The gas starts to dissolve into the liquid immediately after entering the autoclave and the system pressure decreases until it reaches the thermodynamic equilibrium at pressure $p_{a,1}$. The difference between $p_{rc,1}$ and $p_{a,1}$ is used to calculate the number of moles of the gas dissolved in the liquid $N_{dissolved}$ by subtracting the moles of gas remaining in the gas phase at the end of the measurement from the total amount of gas entered into the autoclave at the beginning of the experiment ($N_{rc\rightarrow a}$). During chemisorption measurements gas is added to the autoclave multiple times and the number of dissolved gas molecules is summarized for determination of chemical CO_2 loading capacity B_i.

For calculating the number of moles in the gas phase, Peng Robinson equation of state is applied. Before applying the system for determining the gas solubility in IL it was validated via measurements of CO_2 and CH_4 solubility in water. Any data point referred to in this work was reproduced at least three times.

Physical absorption of CO_2 and CH_4 in RTIL

Gas solubility of a poorly soluble gas i in a liquid j by means of physical absorption (no chemical reaction takes place in the liquid phase) can be expressed in terms of the Henry coefficient H_{ij}, as defined in Eq. (2):

$$H_{ij}(T) = \frac{p_i}{x_i} \tag{2}$$

In Eq. (2), p_i represents the partial pressure of the gas i in the gas phase. x_i is the molar fraction of gas i dissolved in the liquid phase. In all measurements the CO_2 partial pressure in the autoclave was considerably lower than 10 bar, ideal behavior in g and l phase can be assumed.

The solubility is a result of molecular interactions between the solute and the solvent. Considering the gas molecules, CO_2 features a quadrupole moment and is therefore able to interact with polar solvents. It is known from literature that the solubility of CO_2 can be enhanced by adding polar groups to the solvents' molecules. Due to their polar structure, IL feature a high solubility for CO_2 (see Fig. 11).

Methane is a non-polar molecule and is therefore not attracted by any polar groups or dispersion forces present within the solvents molecules. In accordance with the literature findings the solubility of methane in the tested IL is significantly lower than the CO_2 solubility (see Fig. 12).

Besides, any dissolved gas molecule needs to be embedded within the solvent molecules matrices. Therefore, the gas solubility is high in rather large and branch solvent molecules, as the comparison of experimental CO_2 solubility in [EMIM] and [BMIM] IL (also shown in Fig. 11) reveals (see also Fig. 13). Unfortunately, this kind of solubility

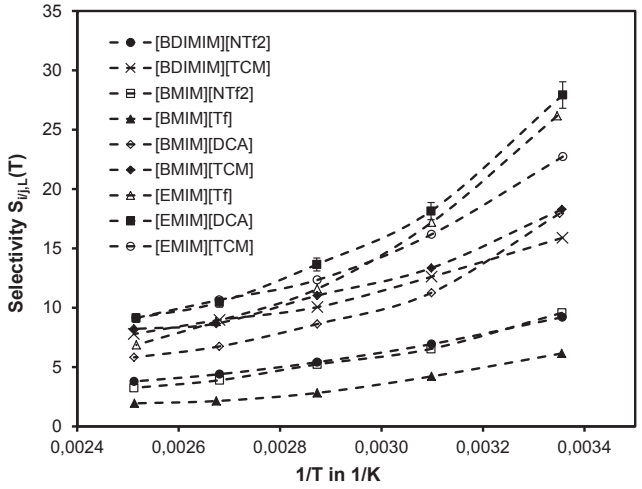

Fig. 13. Low pressure CO_2/CH_4 selectivity S_{CO_2}/CH_4,j in [BDiMIM], [BMIM] and [EMIM] IL with [NTf_2], [TCM], [Tf] and [DCA] anions at 25 < T < 125 °C.

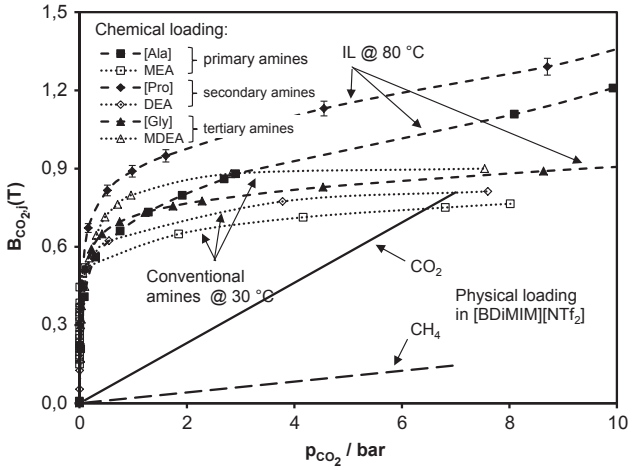

Fig. 14. Comparison of CO_2 solubility of conv. Amines (30 °C; 30 wt% in water): MEA, DEA, MDEA; Corresponding IL (80 °C; 10 wt% in [BDiMIM][NTf_2]): [BDiMIM][Ala], [BDiMIM] Pro], [BDiMIM][Gly] + PZ in a ratio of 2:1); Physical solubility of CO_2 and CH_4 in [BDiMIM][NTf_2] at T = 80 °C.

Table 8
Parameters of Eq.3 (Δh_0 and $\ln(H_{ij,0})$).

RTIL	CO_2		CH_4	
	Δh_0/kJ·mol^{-1}	$\ln(H_{CO2,j,0})$	Δh_0/kJ·mol^{-1}	$\ln(H_{CH4,j,0})$
[BDIMIM][NTf_2]	11.39	8.34	3.93	7.51
[BDIMIM][TCM]	11.22	8.34	4.21	8.26
[BMIM][NTf_2]	13.93	9.24	3.3	7.19
[BMIM][Tf]	14.66	9.9	2.74	6.88
[BMIM][DCA]	13.13	9.67	2.07	8.03
[BMIM][TCM]	11.63	8.67	3.58	8.3
[EMIM][Tf]	14.11	9.73	1.06	7.72
[EMIM][DCA]	12.46	9.37	1.33	8.17
[EMIM][TCM]	11.5	8.72	2.54	8.19

improvement favors non-selective absorption causing co-absorption of methane and resulting in CH_4 loss during gas upgrading.

The temperature dependency of solubility of CO_2 and CH_4 in the tested IL can be described by Eq. (3). H_{ij} represents the Henry's law constant of the gas i in the liquid j in bar, $\ln(H_{ij,0})$ the ordinate intercept ($1/T \rightarrow 0$) and Δh_0 represents the enthalpy of solution. The obtained parameters are summarized in Table 8. With Eq. (4), the solubility of CO_2 and CH_4 can be calculated within the experimental temperature range of 298.15 K ≤ T ≤ 398.15 K.

$$\ln(H_{ij}(T)) = \ln(H_{ij,0}) - \frac{\Delta h_0}{R\Delta T} \quad (3)$$

At 25 °C the selectivity S_{CO_2}/CH_4,j (= H_{CH_4},j/H_{CO_2},j) of all [EMIM] based [TCM], [DCA] and [Tf] based RTIL is in the range of 22–28 (see Fig. 13). For comparison, due to it's polar nature, the selectivity S_{CO_2}/CH_4,H_2O(25 °C) in water is in the same range (≈24 [53–55]), while in common polyethylene glycol (PEG) based solvents for biogas upgrading the selectivity S_{CO_2}/CH_4,PEG–DME(25 °C) is significantly lower (ca. 13 [55,56]). [BMIM] RTIL, especially with [NTf_2] anions, suffer a lower selectivity, caused by the branch structure of the cation and the anion, respectively.

With an increase of temperature selectivity reduces as the CO_2 solubility decreases. The solubility of methane shows only a slight decrease with temperature. It is known from literature that certain gases show only weak temperature dependency of solubility (e.g. CH_4, N_2) or even feature an increase of solubility with temperature (e.g. H_2).

This is also valid for RTIL. In literature, the inversion of temperature dependence is described as a consequence of an enthalpy-entropy compensation issue [57]. Strong interacting solutes feature a negative enthalpy of solution (exothermic solvation) but also a negative entropy of solution. At a certain temperature strongly interacting gases pass through a minimum of excess solution energy, where enthalpy of solvation and entropic contribution to the solvation process equal out (this point is a solubility minimum). There are only few explanations for the entropy contribution present: It is assumed that the solute influences the order of the solvent molecules or possibly reduces the degree of freedom of solvent molecules movement.

Chemical absorption of CO_2 in CFIL

When chemical absorption takes place the chemical loading capacity B of CO_2 (see Eq. (4)) in the solvent is typically dominated by the stoichiometry of the chemical reaction. Methane is chemically inert, only CO_2 is able to participate in the chemical reaction. Therefore, the absorption is typically operated at ambient pressure and a significantly higher selectivity ($S_{CO2/CH4,L} > 100$) is achieved.

$$B_{ij}(T) = \frac{N_i}{N_{amine\ groups\ in\ the\ solvent\ j}} \quad (4)$$

Fig. 14 shows a comparison of experimental solubility results of common aqueous amine solutions (all 30 wt% in water) at 30 °C vs. 10 wt% CFIL in [BDiMIM][NTf_2] at 80 °C.

As expected, conventional solvents show an increase of solubility from primary to tertiary amines (see Table 2). Any of the applied conventional amines show a higher CO_2 capacity B_{CO2} than 0.5 as the general Eq. (5) of the reaction of CO_2 with primary and secondary amines allows:

$$2R{-}NH_2 + CO_2 \rightleftharpoons R{-}NH_3^+ + R{-}NH{-}COO^- \quad (5)$$

This is induced by water participating in the reaction when high CO_2 partial pressures are applied: When R-NH-COO^- concentration reaches the value of 0.5 certain amounts of HCO_3^- are reversely formed from the carbamate (Eq. (6)), with R-NH_2 again acting as base for CO_2 uptake (via H_3O^+ neutralization, see Eqs. (7), (8) and Fig. 15).

$$R{-}NH{-}COO^- + H_2O \rightleftharpoons R{-}NH_2 + HCO_3^- \quad (6)$$

$$CO_2 + 2H_2O \rightleftharpoons H_3O^+ + HCO_3^- \quad (7)$$

$$R{-}NH_2 + H_3O^+ \rightleftharpoons R{-}NH_3^+ + H_2O \quad (8)$$

Obviously, in dry amines the capacity B_i would be limited to 0.5. When applying tertiary amines (e.g. MDEA), the CO_2 uptake invariably takes place by storing CO_2 as HCO_3^-. The amine exclusively serves as a base and CO_2 capacities of 1 mol of CO_2 per mol of MDEA are possible.

In contrast to conventional amine solutions, in this work the CFIL are applied as dry mixtures with RTIL. RTIL do not participate in the

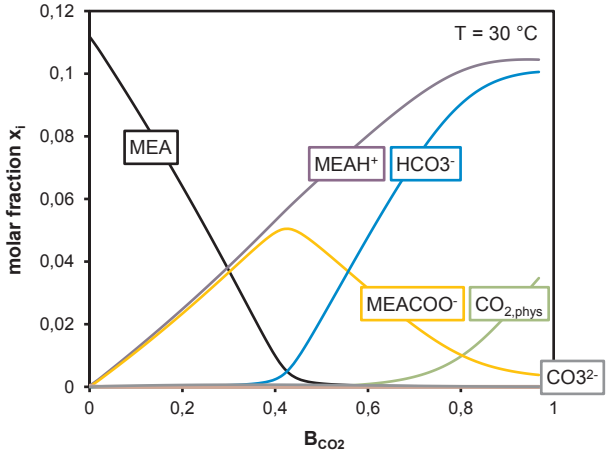

Fig. 15. ASPEN simulation results of species distribution x_i in 30 wt% aqueous MEA solution at T = 30 °C as a function of overall CO_2 loading (OH^-, $H_3O^+ \approx 0$).

chemical reaction. For the primary and secondary amino-acid based anions alaninate [Ala] and prolinate [Pro] a maximum capacity of 0.5 is expected (similar to Eq. (5)) in absence of water.

Nevertheless, it is already known from literature and also observed in the experiments in this work (see Fig. 14), that higher CO_2 loadings, even close to 1 mol CO_2 per mole of amine-functionalized anion are possible with CFIL. Chemical complexation of protons in the solvent or rather consecutive reaction of the carboxylates to the corresponding acids, or carboxylation of the (2)-position at the imidazole ring are discussed as reasons for this evidence.

In any of the experiments shown in Fig. 14, the corresponding cation was [BDiMIM], in CFIL as well as in RTIL. Therefore, the (2) position of the imidazolium did not participate in CO_2 absorption chemistry as it was already alkylated. Chemical complexation or rather consecutive formation of the corresponding acids may still occur. For further identification unused and CO_2 saturated samples of the IL mixtures were analyzed by ^{1}H- and ^{13}C-NMR.

NMR results of [BDiMIM] [Pro] loaded with CO_2

The ^{1}H- and ^{13}C-NMR of the unused mixture of [BDiMIM][NTf_2] with 30 wt% [BDiMIM][Pro] shows the expected peaks and intensities for this mixture. The intensity of the NH-peak with approximately 0.5 fits well to 30 wt% prolinate. The unused sample was therefore identified as [BDiMIM][Pro].

In addition to the unused mixture of the ionic liquids, NMR-spectra were also measured after loading the mixture with 0.075, 0.244 and 0.46 mol carbon dioxide per mol prolinate. In the ^{1}H NMR of the loaded mixture with 0.075 mol carbon dioxide the intensity of the NH-peak is reduced significantly. In addition, the resolution of the CH-peak at 3.2 ppm degrades. Together with a new ^{13}C-peak at 160 ppm, which fits with N-COO, this is a strong evidence that the prolinate reacts with carbon dioxide under formation of pyrrolidine-1,2-dicarboxylate. From the NMR measurements it was not possible to identify any group containing the free proton. Therefore, it can be assumed that the proton is weakly stabilized complexation by the carboxylate groups in the mixture.

Increasing the CO_2 load to 0.224 mol/mol prolinate, no NH-peak is observed in the ^{1}H NMR anymore and the resolution of the CH-peaks of prolinate at 3.2 ppm and 1.8 ppm is reduced even more. Looking at the ^{13}C NMR the intensity of the N-COO peak is higher than after loading the mixture with 0.075 mol CO_2. In addition the signals of the CH_2-peaks of the prolinate at 30 and 31 ppm is wider than for the unused mixture. Increasing the CO_2 load to 0.46 mol/mol prolinate, the ^{1}H NMR shows still no NH-peak of the prolinate anymore and the resolution of the peaks at 3.2 ppm and 1.8 ppm is even less. The N-COO-peak at 160 ppm has the highest intensity of all discussed ^{13}C-spectra. This again accounts for CO_2 reacting with the prolinate anion under formation of pyrrolidine-1,2-dicarboxylate and the proton being complexated in the liquid phase.

Fig. 14 further shows that the CO_2 capacity increases from primary to secondary amino acid based anions. The primary and secondary amino acid based anions are able to capture CO_2 directly via carbamate formation. The dimethylglycinate anion can only act as proton acceptor. CO_2 fixation must take place elsewhere. Therefore, (in absence of any water) piperazine (a cyclical bi functionalized secondary amine) was added to the solvent system, which is able to form the carbamate when reacting with CO_2. The residual CO_2 capacity of the dimethylglycinate based CFIL is in the same range as for the alalinate IL. Applying tertiary amines in dry IL systems therefore provides no additional benefit. As the thermal stability of the dimethylglycinate based IL is rather unsatisfactory and piperazine dissolution in the examined dimethylgylcinate based IL mixture is inadequate, the prolinate based IL was chosen as best option for the specified task out of the tested IL and therefore further characterized.

For comparison reasons, the physical solubility of the applied RTIL [BDiMIM][NTf_2] was added to Fig. 14. As can be seen, the chemical solubility of CO_2 at p_{CO_2} = 0.5 bar is 14 times larger than the physical solubility. Furthermore the selectivity of dissolved CO_2 (chemically and physically) to dissolved CH_4 is in the range of 50, which is comparably low for chemical solvents but can be further optimized by increasing the concentration of CFIL in the mixture or by substituting [BDiMIM][NTf_2] by an RTIL with a lower methane solubility, e.g. by a [TCM] anion based RTIL.

Fig. 16 shows the effect of temperature on chemical CO_2 loading. Equivalent to common amines the isotherms shift to lower CO_2 loadings with an increase of temperature due to the exothermic reaction. For further process efficiency calculations, a temperature dependent equilibrium constant was evaluated. As the proportion of protonated amine groups to chemically complexated protons in the liquid is unknown, the stoichiometry of the reaction cannot be given. Therefore a stoichiometry factor X (see Eq. (10)) was incorporated to the fit of the experimental results via minimization of least squares. X represents the necessary number of moles of unreacted amines for fixation of one mole of CO_2 (see Eq. (9)). The calculations result in X = 1.68, which is in between the minimum stoichiometry of 0.5 mol of CO_2 per mole of amines (corresponding to X = 2) and a 1:1 stoichiometry.

For the temperature dependence of K(T), Eq. (11) was applied. Comparison of experimental results and K(T) predictions is shown in Fig. 16. With the given equation the chemical absorption capacity of CO_2 in [BDiMIM][Pro] can be determined in the range of $p_{CO2} \leq 1$ bar and 60 °C ≤ T ≤ 120 °C with sufficient accuracy.

$$XR{-}NH_2 + CO_2 \rightarrow RNCOO + (X{-}1)RNH_2 \times H^+ \quad (9)$$

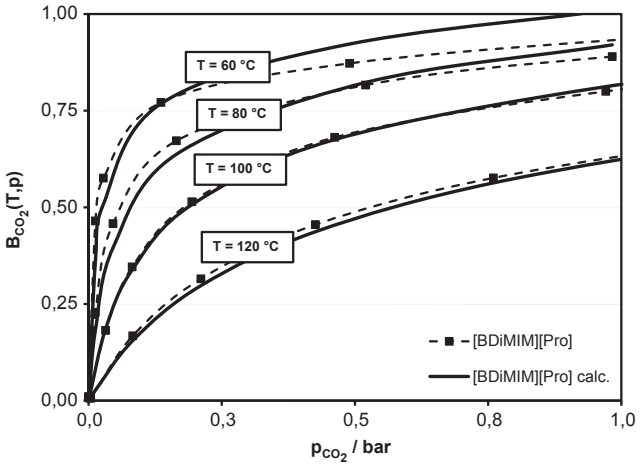

Fig. 16. Effect of temperature variation on the chemical loading capacity of 10 wt% [BDiMIM][Pro] in [BDiMIM][NTf_2].

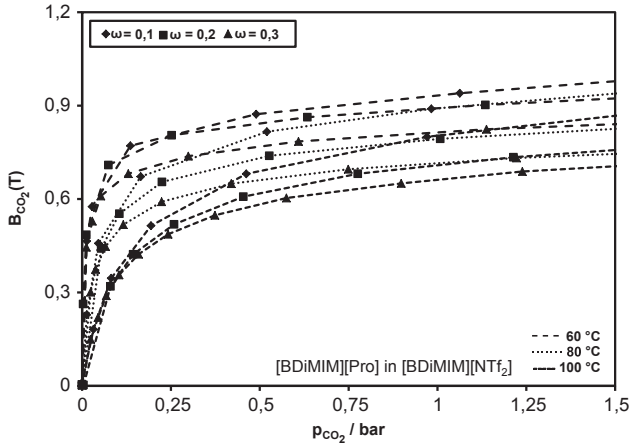

Fig. 17. Variation of mass fraction of [BDiMIM][Pro] in [BDiMIM][NTf_2] in the temperature range of 60–100 °C.

$$K = \frac{c_{CO_2,chem}}{c^{X}_{amine} \cdot c_{CO_2,phys}} \tag{10}$$

$$K(T) = \exp\left(-8.471 + \frac{5348.7}{T}\right) \tag{11}$$

Fig. 17 shows a variation of mass fraction of the chemical active compound [BDiMIM][Pro] in [BDiMIM][NTf_2]. In the range of very low CO_2 partial pressures ($p_{CO_2} \rightarrow 0$), chemical absorption dominates the CO_2 capacity curves. In this pressure range the specific amount of CO_2 captured per mole of applied amine is fairly equal by means of double and three times as much CO_2 has been absorbed into the liquid for 20 wt% and 30 wt%, respectively.

For higher pressures the CO_2 capacity curves spread: the slope of the curves decline with an increase of [BDiMIM][Pro] fraction in the solvent. As the physical solubility of CO_2 in [BDiMIM][Pro] is lower than in [BDiMIM][NTf_2], higher fractions of [BDiMIM][Pro] lead to less physically absorbed CO_2.

Finally, the effect of admixing of water on CO_2 solubility was examined, see Fig. 18. Water can be an issue for a potential technical process as nearly any completely dry IL behaves hygroscopic. Therefore, when contacted with water a certain amount of water will accumulate in the solvent cycle. By adding 5 wt% of water to the solvent mixture the CO_2 capacity reduces sharply. This finding might be a result of water reducing the amount of complexated protons in the solution or by participating in CO_2 absorption by direct formation of carbonate, releasing two additional protons.

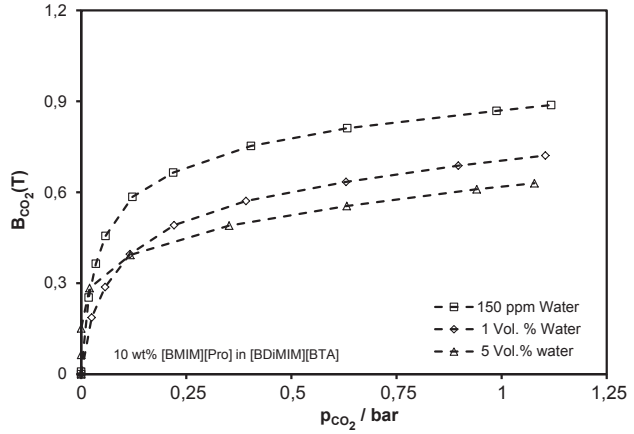

Fig. 18. Influence of water on the CO_2 capture ability of the IL solvent mixture (10 wt% [BDiMIM][Pro] in [BDiMIM][NTf_2]) at T = 80 °C.

3.3. Effective and intrinsic rate of CO_2 absorption

For CO_2 removal via gas scrubbing not only CO_2 loading capacity but also absorption kinetics is an important solvent property, as the size of a gas/liquid contact apparatus is typically determined by how fast the gas impurities are dissolved in the liquid.

In general, a distinction between the effective and the intrinsic rate of absorption can be drawn. The effective absorption rate is the more important parameter as it defines the size of the mass transfer apparatus. Conversely, the effective rate is closely linked to the applied apparatus, as not only reaction kinetics but also e.g. mass transfer contributes to the overall performance.

However, the intrinsic absorption rate represents the rate of chemical reaction between CO_2 and the solvent and therefore is a fundamental solvent property which can be transferred from one reactor design to another, e.g. from lab scale autoclave (as applied in this work, see Fig. 10) to a technical scale absorption column.

Effective rate of absorption

In order to compare the effective kinetics of the tested ionic liquids, equivalent rate experiments were conducted with conventional solvents MEA, DEA, MDEA and MDEA + PZ, each 30 wt% of the amines in water.

In the applied setup CO_2 is absorbed from the gas phase into a stirred liquid phase (see Fig. 10). Before CO_2 can chemically react with any amines in the liquid phase it has to be absorbed at the phase interface and then physically transported to the reactive species. The result of these consecutive steps is referred to as the effective absorption rate in terms of the decline of the system pressure in the autoclave as a function of time (see Eq. (12)).

$$\frac{dp_{CO_2}}{dt} = \frac{RT_G}{V_G} \beta_{CO_2,L} \cdot A \cdot E \cdot (c^{*}_{CO_2,L} - c_{CO_2,L,\infty}) \tag{12}$$

with $\beta_{CO_2,L}$: physical mass transfer coefficient
$E = (\beta_{CO_2,L} \cdot A)_{effective} / (\beta_{CO_2,L} \cdot A)_{without\ chemical\ reaction}$
$c^{*}_{CO_2,L}$: equilibrium concentration at phase boundary
$c_{CO_2,L,\infty}$: concentration in the bulk liquid.

The autoclave is operated at a gas to liquid ratio of 3–4. The initial pressure $p_{CO2,0}$ was chosen to 30×10^{-3} bar in order to minimize temperature changes in the gas phase by Joule Thompson effect, temperature variations in the liquid phase by the exothermal chemical reaction and to avoid depletion of amine at the phase interface during reaction.

Fig. 19 shows the experimental results for the effective absorption rate of the mentioned amine systems. The slope of the pressure curves (see Eq. (12)) represents the effective absorption rate. As expected and often reported in literature, MEA features a very fast effective absorption rate. When 30 wt% of MEA are applied it takes approximately 30 s to absorb the CO_2 from the gas phase completely, i.e. the remaining partial pressure of CO_2 equals zero. The $DEA_{(aq)}$ system is slower. $MDEA_{(aq)}$ without PZ is by far the slowest, even in comparison to the ionic liquids. MDEA with addition of PZ again shows equal performance as MEA. Bishnoi et al. [58] proposed, that the absorption rate of a pure aqueous PZ solution is much faster than an aqueous MEA solution. The authors observed that multi-amines and cyclic molecule structures enhance the reaction rate. The fact that the reaction rate of a mixture of $MDEA_{(aq)}$ + $PZ_{(aq)}$ is as fast as aqueous MEA is caused by the protonation reaction of the amine which is the overall rate determining step.

The experimental results of the examined IL systems are also included in Fig. 19. As it is known from literature, low temperatures are critical for the performance of ionic liquids due to their elevated viscosity. The RTIL [BDiMIM][NTf_2] features a viscosity of 25×10^{-3} Pa s at 60 °C, which is 23 times higher than the aqueous MEA system. But still, the [Ala] based mixture shows equal effective absorption

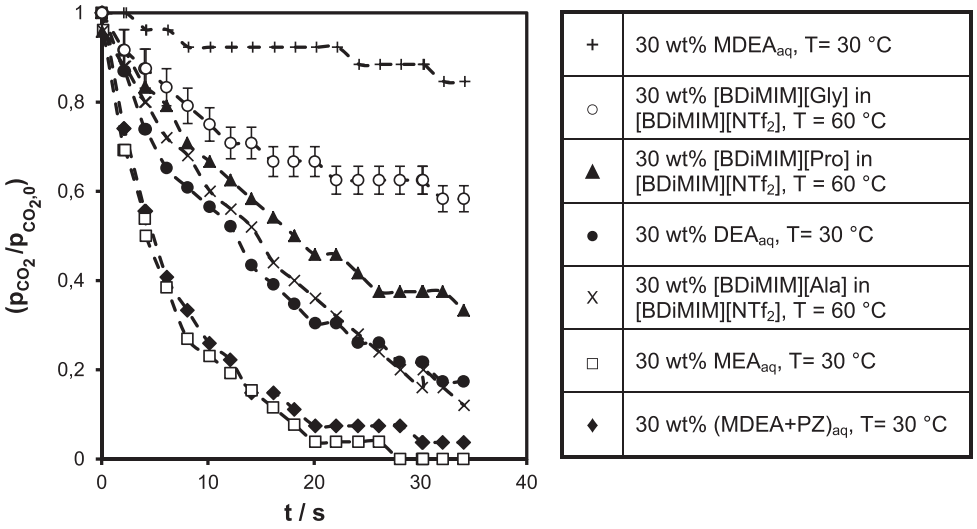

Fig. 19. Normalized pressure decrease by CO_2 absorption for different conventional amines and functionalized ionic liquid mixtures.

performance than the aqueous DEA solvent, the [Pro] based IL is only slightly slower. This indicates that the examined IL based solvents feature a relatively good mass transfer performance, which is fast enough to apply the tested IL to CO_2 separation in technical scale.

The experiment indicates that the size of the necessary mass transfer columns will probably be in the same order of magnitude for the IL based solvents in the optimized separation process operated at approximately 60–80 °C as for the conventional aqueous secondary amine based CO_2 separation processes.

Fig. 20 shows that the contrarious reactions of solvent regeneration of secondary amines start to take place at temperatures of approximately 50–60 °C, decelerating the effective rate of CO_2 absorption. This implies that a regeneration of the solvents is possible at temperatures above 60 °C.

Nevertheless, in most of the cases (except at the very high temperatures), CO_2 was completely absorbed into the liquid phase, indicating that the reduction of the effective rate of absorption was not limited by thermodynamic equilibrium.

Intrinsic rate of absorption

In continuous operation, the mass balance of CO_2 in the liquid film can be expressed by Eq. (13), assuming a second order reaction of CO_2 with the amine species. In case the amine is present in large excess (as it was during the absorption rate measurements), it is not necessary to consider the concentration of the amine species in the liquid phase ($c_{amine,L}$ = const.). Therefore, in the CO_2 balance the concentration of the amine species and rate constant k may be combined to a pseudo first-order reaction rate equation (Eq. (14)).

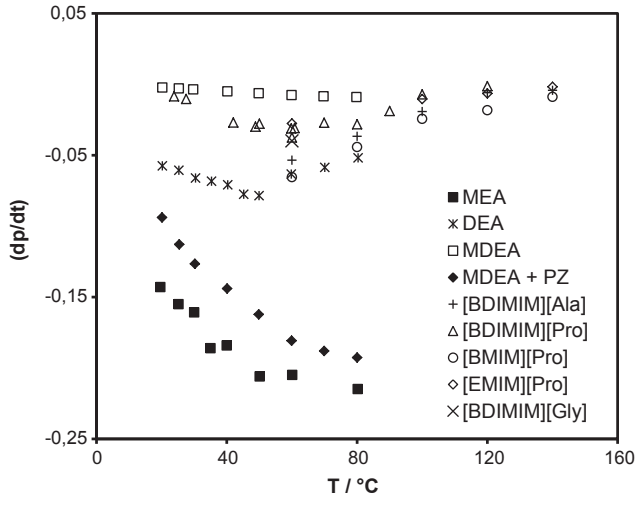

Fig. 20. Slope of Eq. (12) for various tested solvent systems as a function of temperature.

$$\underbrace{D_{CO_2,L}\frac{\delta^2 c_{CO_2,L}}{\delta y^2}}_{J_{CO_2,G\to L}} - r_{CO_2,L} = 0 \tag{13}$$

$$r_{CO_2,L} = \frac{1}{V_L}\frac{dn_{CO_2}}{dt} = k\cdot c_{amine,L}\cdot c_{CO_2,L} = k\cdot c_{CO_2,L}c \tag{14}$$

Integration of Eq. (13) yields the concentration profile of CO_2 in the liquid film layer, Eq. (15). δ_L represents the thickness of the liquid film. $c^*_{CO_2,L}$ represents the CO_2 concentration in the liquid directly at the gas-liquid interface. $c_{CO_2,L,\infty}$ is the CO_2 concentration in the bulk liquid phase.

$$c_{CO_2,L}(y) = \frac{c^*_{CO_2,L}\sinh\left(Ha\left(1-\frac{y}{\delta_L}\right)\right) + c_{CO_2,L,\infty}\sinh\left(Ha\frac{y}{\delta_L}\right)}{\sinh(Ha)} \tag{15}$$

Ha represents the proportion of maximum chemical conversion rate to maximum physical mass transfer rate by diffusion in the liquid film layer. Eq. (16) shows the simplified definition of *Ha* for first order reactions.

$$Ha = \delta_L\sqrt{\frac{k'}{D_{CO_2,L}}} = \frac{1}{\beta_{CO_2,L}}\sqrt{k'D_{CO_2,L}} \tag{16}$$

For fast reactions, e.g. the chemical reaction of CO_2 with amines, $Ha > 3$, meaning that the reaction takes place exclusively in the liquid film layer or even instantaneous at the phase interface. Therefore, the concentration of CO_2 in the bulk liquid phase $c_{CO2,L\infty} \approx 0$ and the chemical enhancement factor is maximized: $E \approx Ha$. In this case, Eqs. 12, 14 and 16 can be combined to Eq. (17).

$$\int\frac{1}{p_{CO_2}}dp_{CO_2} = \int\frac{ART_G}{V_G H_{CO_2,L}}\sqrt{kD_{CO_2,L}}\,dt \tag{17}$$

With Eq. (17), it is possible to evaluate the reaction specific rate constant k′ from the experimental measurements and therefore the intrinsic kinetics of the CO_2 absorption reaction when the solubility of CO_2 and the diffusion coefficient of CO_2 in the liquid are known. The latter has been measured via N_2O analogy [59] in [BDiMIM][NTf_2] and is given by Eq. (18). For simplification, the effect of admixing the CFIL into the RTIL on the diffusion coefficient was neglected.

$$\frac{D_{CO_2,L}(T)}{10^{-9}\ \mathrm{m\ s^{-1}}} = -1514\frac{1}{T} + 5.42 \tag{18}$$

Fig. 21 shows the results for the for tested conventional solvents

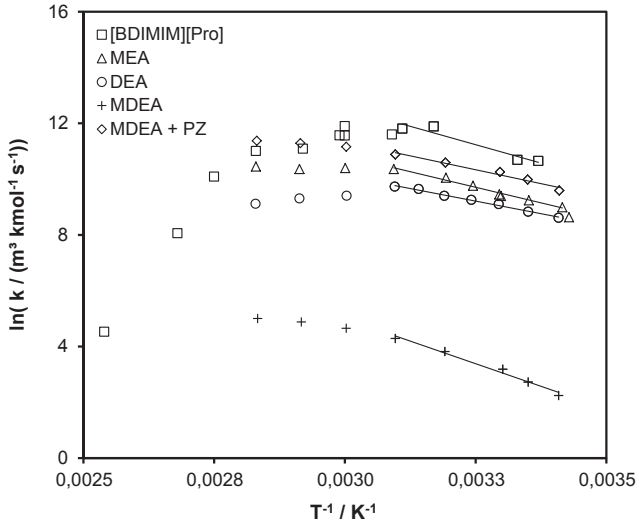

Fig. 21. k of second order reaction of CO_2 with various amine solvents.

Table 10
Heats of CO_2 absorption Δh of conventional solvents and CFIL.

Solvent	Δh_{exp}/ kJ·mol^{-1}	Δh_{Lit}/ kJ·mol^{-1}	Measurement temperature/°C
$MEA_{(aq,\ \omega\ =\ 30\%)}$	83.8	85 [16,64]	25
$DEA_{(aq,\ \omega\ =\ 30\%)}$	70.9	70.4 [64]	25
$MDEA_{(aq,\ \omega\ =\ 30\%)}$	–	58.8 [65]	25
$MDEA + PZ_{(aq,\ 2:1,\ \omega\ =\ 30\%)}$	–	77 [66]	25
$[BDiMIM][Ala]_{(\omega\ =\ 10\%)}$	101.7	–	90
$[BDiMIM][Pro]_{(\omega\ =\ 10\%)}$	80.2	–	90

$MEA_{(aq)}$, $DEA_{(aq)}$, $MDEA_{(aq)}$ and $MDEA + PZ_{(aq)}$, 30 wt% amine each, and the ionic liquid system 10 wt% [BDiMIM][Pro] in $[BDiMIM][NTf_2]$.

As can be seen in Fig. 21, the prolinate based IL solvent features the highest intrinsic reaction rate of all tested solvents. Besides simplifications in calculation of the diffusion coefficient, this might be induced by a high specific heat of reaction (see Section 3.4) which typically

Table 9
Calculated k′, k, ln(k_0), E_A and $E_{A\ Lit.}$ of the reference systems and [BDiMIM][Pro] in $[BDiMIM][NTf_2]$ at various temperatures.

		MEA						DEA					
		k′ × 10^{-3}/s^{-1}	k × 10^{-3}/ m^3 kmol^{-1} s^{-1}	ln(k)	ln(k_0)	E_A/kJ·mol^{-1}	E_A Lit./ kJ·mol^{-1}	k′ × 10^{-3}/s^{-1}	k × 10^{-3}/ m^3 kmol^{-1} s^{-1}	ln(k)	ln(k_0)	E_A/kJ·mol^{-1}	E_A Lit./ kJ·mol^{-1}
T in °C	20	40.03	8.05	8.99	27.05	44.32	44.94 [60]	16,289.57	5506.16	8.61	21.41	31.17	32.3 [61]
	25	51.22	10.32	9.24				20,218.91	6852.80	8.83			
	30	59.76	12.07	9.40				26,437.24	8984.65	9.10			
	35	85.74	17.36	9.76				30,768.57	10,456.64	9.25			
	40	114.04	23.14	10.05				35,606.86	12,100.92	9.40			
	45	–	–	–				45,309.73	15,440.24	9.64			
	50	155.25	31.67	10.36				49,332.57	16,811.10	9.73			
	60	159.76	32.78	10.40				35,150.64	12,143.17	9.40			
	70	153.14	31.62	10.36				32,204.18	11,004.13	9.31			
	80	167.79	34.65	10.45				26,581.58	9107.69	9.12			

		MDEA						MDEA + PZ					
		k′ × 10^{-3}/s^{-1}	k × 10^{-3}/ m^3 kmol^{-1} s^{-1}	ln(k)	ln(k_0)	E_A/kJ·mol^{-1}	E_A Lit./ kJ·mol^{-1}	k′ × 10^{-3}/s^{-1}	k × 10^{-3}/ m^3 kmol^{-1} s^{-1}	ln(k)	ln(k_0)	E_A/kJ·mol^{-1}	E_A Lit./ kJ·mol^{-1}
	20	24.50	9.44	2.24	22.46	48.9	45 [62]	41.69	14.62	9.59	25.06	33.11	33.75 [63]
	25	39.58	15.30	2.73				61.61	21.65	9.98			
	30	62.38	24.19	3.19				80.78	28.47	10.26			
	35	–											
	40	117.82	45.69	3.82				112.21	39.75	10.59			
	45	–	–	–				–	–	–			
	50	188.10	72.94					149.56	53.26	10.88			
	60	270.31	105.17					196.11	70.21	11.16			
	70	338.46	131.69					221.67	79.78	11.29			
	80	376.99	149.14					240.25	86.93	11.37			

	10 wt% [BDiMIM][Pro] in $[BDiMIM][NTf_2]$					
	k′ × 10^{-3}/s^{-1}	k × 10^{-3}/ m^3 kmol^{-1} s^{-1}	ln(k)	ln(k_0)	E_A/kJ·mol^{-1}	E_A Lit./ kJ·mol^{-1}
25	22.5	42.31	10.65	28.37	43.83	–
30	23.38	44.05	10.69			
40	76.74	145.97	11.89			
50	70.74	135.15	11.81			
60	76.26	146.86	11.9			
70	33.78	65.48	11.09			
80	31.08	60.66	11.01			
90	12.28	24.13	10.09			
100	1.6	3.17	8.06			
120	0.047	0.093	4.53			

enhances the chemical reaction rate (see Tables 9 and 10).

3.4. Heat of reaction

The specific heat of reaction Δh of the applied CFIL during CO_2 absorption were measured with a STA 409CD microbalance from Netzsch-Gerätebau GmbH and compared to measurements and literature values of conventional amine based solvents ($MEA_{(aq)}$, $DEA_{(aq)}$, MDEA + $PZ_{(aq)}$). Due to the high viscosities of the applied ionic liquids the measurements with IL have not been carried out at standard conditions. In comparison to conventional amines all applied ionic liquids show an increased heat of reaction. This has already been expected from the results of reaction kinetics and CO_2 uptake, as both are rather high in comparison to conventional amines.

4. Process efficiency estimation

Based on the characterization of the IL solvent, a first efficiency estimation of the proposed process was carried out by calculating the thermal and the electrical energy demand and comparing it to state-of-the-art technologies for biogas upgrading. The flow sheet of the upgrading process is given in Fig. 22.

The calculations are based on the following boundaries and simplifications:

- Feed volume flow is 1000 m^3/h (25 °C) with $y_{CO2,in} = y_{CH4,in} = 0.5$
- The raw biogas temperature at the inlet of the scrubbing unit is 35 °C
- For heat capacity and density of the CFIL mixture, the values of the RTIL are applied
- The absorption temperature is equal to the temperature of the desorption (80 °C)
- The minimum temperature difference in any heat exchangers is $\Delta T_{min} = 10$ °C
- The methane content at the outlet of the absorption column is $y_{CH4} > 0.95$
- Heat losses to the ambient are neglected
- Vacuum (200 mbar in Col-02 and 50 mbar in Col-03) is applied via roots pump (C01/02) (isochoric operation)
- The efficiency of energy transformation: primary to thermal is 0.9 and primary to electrical energy is 0.42 [67] (which is the average efficiency of German power supply).

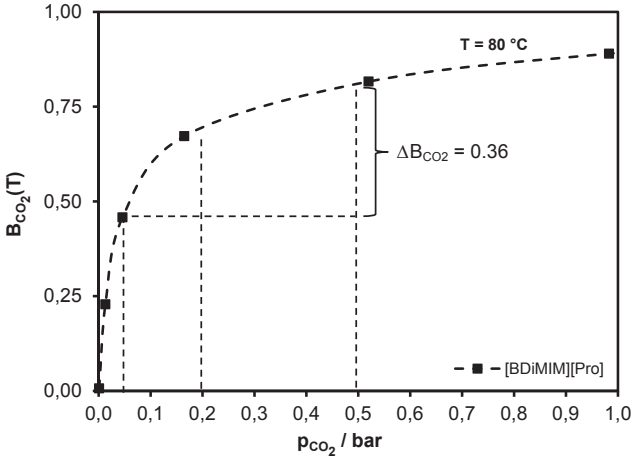

Fig. 23. 10 wt% [BDiMIM][Pro] in [BDiMIM][NTf_2] isotherm and corresponding loading capacities per liquid cycle ΔB_{CO2}.

Table 11
Mass balance of the proposed process for 1000 m^3/h (25 °C) raw biogas input.

Mass flows/t·h^{-1} (see Fig. 22)							
$F_{m,RG}$	$F_{m,L1}$	$F_{m,L2}$	$F_{m,L3}$	$F_{m,LG1}$	$F_{m,LG2}$	$F_{m,LG3}$	$F_{m,BG}$
1.17	270	160	110	0.86	0.41	0.45	0.31

The liquid circulation rate can be calculated from the loading capacity isotherms (80 °C in Fig. 23) and the CO_2 partial pressures in the regeneration units (200 mbar in Col-02 and 50 mbar in Col-03), respectively. In total a ΔB of 0.36 can be achieved under these conditions, divided to $F_{m,LG2}$ and $F_{m,LG3}$ (see Fig. 22).

The mass balance is given in Table 11 for a mixture of 10 wt% [BDiMIM][Pro] in [BDiMIM][NTf_2], resulting in comparably high liquid circulation rates of 270 t/h.

The liquid circulation rate and the selectivity of the RTIL strongly affect the methane loss caused by co-absorption in the liquid. In the calculated case a methane loss of 2.7% occurs with [BDiMIM][NTf_2] caused by the high liquid circulation rate and the low selectivity of the solvent. By applying [BDiMIM][TCM] instead, the methane loss can be

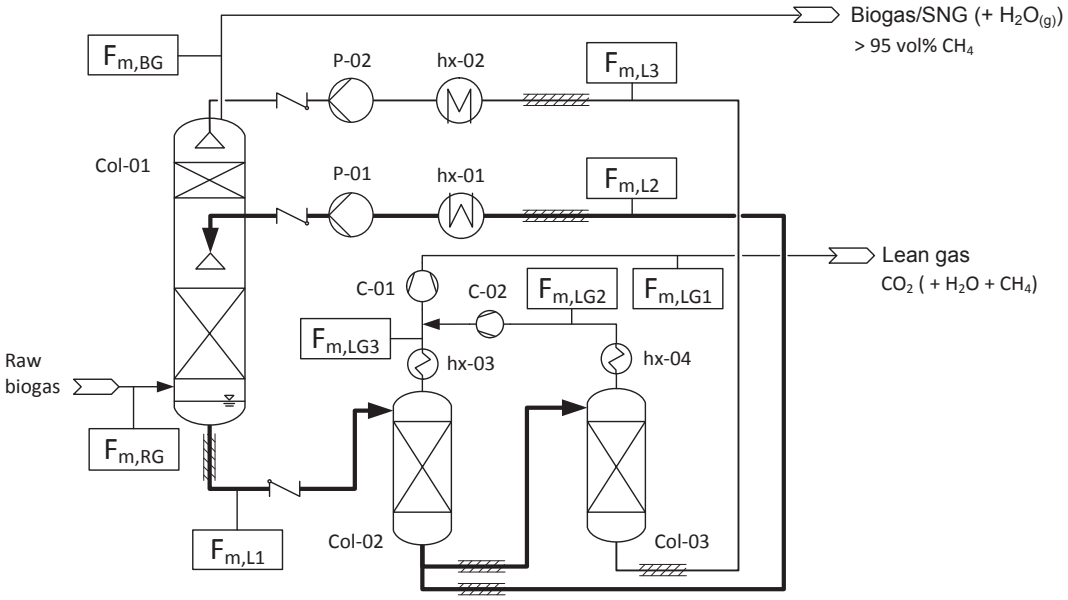

Fig. 22. Proposed process concept with G and L mass flows indicated.

Table 12
Comparison of thermal, electrical and primary energy demand of state-of-the-art technologies for biogas upgrading with the proposed isothermal IL process.

	$e_{thermal}$/ $kWh \cdot m^{-3}_{Rawgas,NTP}$	$e_{electrical}$/ $kWh \cdot m^{-3}_{Rawgas,NTP}$	$e_{primary}$/ $kWh \cdot m^{-3}_{Rawgas,NTP}$
Water scrubber	–	0.23–0.33	0.58–0.8
PSA	–	0.26	0.65
Chemical scrubber	0.6	0.05	0.8
Membrane separation	–	0.2–0.25	0.5–0.6
Quasi isothermal, chemical IL upgrading	0.02	0.09	0.24

reduced to 1.4% due to the higher selectivity of the RTIL. The methane loss can be further reduced by increasing the mass fraction of CFIL in the solvent mixture, ending in a trade-off between mass fraction of CFIL and viscosity of the mixture. 20 wt% of CFIL in the mixture should be possible, again reducing the liquid circulation and therefore the methane loss by a factor of 2. These low amounts of methane in the lean gas (approximately 30–40 kW in total) can be utilized via catalytic combustion and can be applied for supplying the upgrading process with thermal energy for pre-heating of the feed gas and for compensating heat losses to the ambient. A further reduction of the methane loss is therefore not necessary.

Comparing the total energy demand, the proposed IL based scrubbing process requires a larger share of electrical energy as compared to thermal energy. The major share of the required electrical energy is applied for the vacuum pumps (C-01 and C-02) connected to the desorption units. The remaining electric energy is needed for the liquid pumps (P-01 and P-02). Table 12 shows the results of the calculations. As a result, the proposed process enables primary energy savings of 50–75% in comparison to state of the art technologies.

As it is clear that ionic liquids are cost-intensive solvents (and will certainly always remain more expensive than conventional solvents), the proposed process can only be profitable when OPEX savings compensate for the additional solvent costs.

Taking 8000 h of operation per year and an average price for electricity (corporate clients in Germany) of 0.15 € ct/kWh (heat 5 ct/kWh) as a basis, about 120 k€ can potentially be saved per year in comparison to conventional physical upgrading concepts. Compared to chemical scrubbing, these savings can be nearly doubled by additional biomethane production, as heating of the regeneration unit has to be fired by biogas in Germany. Therefore, besides the electricity price, savings also strongly depend on the actual prices received for injection of biomethane into the gas grid (see Fig. 24).

With an average solvent inventory of around 5 l of solvent per m^3/h of raw biogas to be treated in conventional chemical scrubbing plants, 30–60 € per kg of solvent can be saved annually and therefore reinvested for the IL solvent. According to literature prices of approximately 30–50 €/kg [2,68] may be expected when imidazolium based IL are produced in a commercial scale and halides were avoided (e.g. when using [BDiMIM][TCM]). If solvent costs of 65 € per kg were assumed and the solvent inventory was doubled (due to the higher viscosity of the IL), a payback period of less than < 5 years is calculated for the process design proposed in this paper.

5. Summary and conclusion

In this work an alternative process for CO_2 separation based on the application of ionic liquids has been evaluated for upgrading of biogas. The proposed chemical scrubbing process is operated in a “quasi-isothermal” mode, avoiding the demand for thermal energy for regeneration of the solvent from an external source. Instead, the solvent is regenerated by reducing the CO_2 partial pressure in the gas phase of the regenerator by applying moderate vacuum in a pressure range of 50–200 mbar.

The proposed CO_2 separation concept favors ionic liquids (IL) as solvents, as this class of substances features a negligible vapor pressure at temperatures of up to 150 °C. Additionally, the increase of operating temperature helps to compensate for the common disadvantages of IL (high solvent viscosity, low energetic benefits).

Taking the example of biogas upgrading, ionic liquids were screened and an appropriate solvent was developed as a mixture of RTIL and CFIL with separate focus on minimizing the viscosity of the mixture and providing an appropriate chemical CO_2 absorption capacity and effective absorption rate. For the investigations presented [BDiMIM][NTf_2] was used as RTIL. Future optimization options are to switch to [BDiMIM][TCM] to significantly increase the selectivity, to reduce the viscosity of the solvent mixture by a factor of 2 and to avoid halogens. Concerning chemisorption, prolinate [Pro] based CFIL are promising, as

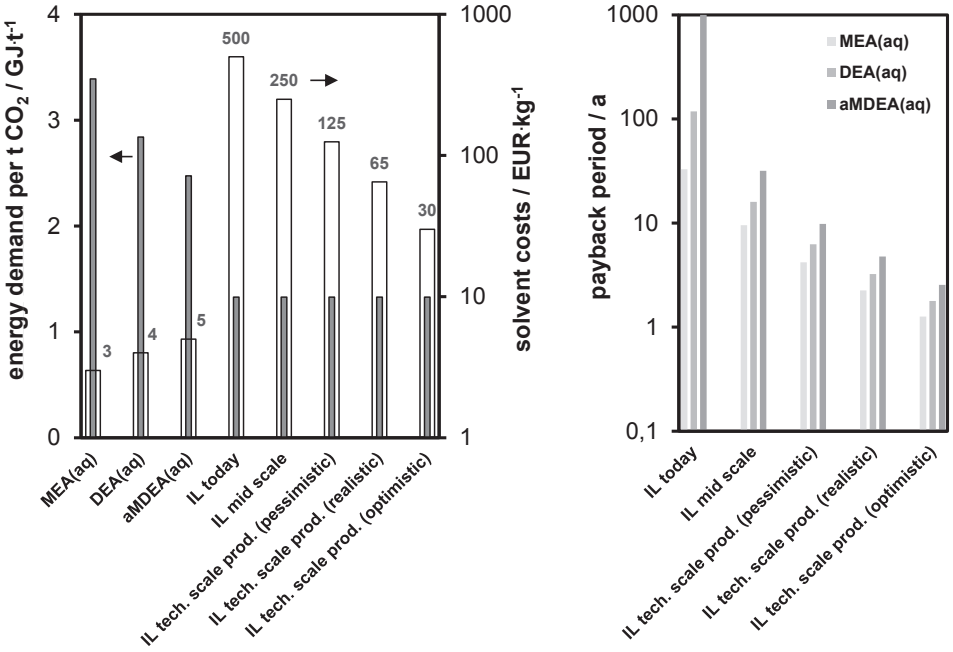

Fig. 24. Results of the economic analysis of the proposed IL based process.

they feature sufficient thermal stability and proper CO_2 loading capacity and kinetics.

During screening and characterization phase, thermal stability, physical CO_2 and CH_4 solubility, effective and intrinsic absorption kinetics, heat of reaction, and additional solvent properties of various examined ionic liquid solvents were evaluated in a temperature range, exceeding the common range of literature values considerably. The measurements on absorption kinetics showed, that the absorption of CO_2 at the desired operating conditions is about as fast as with conventional DEA, which has already been applied for biogas upgrading. From this finding, the conclusion can be drawn that the necessary absorber volume for applying the desired ionic liquid mixture is in the same order of magnitude as for conventional DEA based solvent.

Based on the experimental findings a first process efficiency estimation was performed. As expected from the flow sheet, the major part of the required electrical energy for the process is applied for the vacuum pumps connected to the desorption units. The calculations predict energetic benefits in terms of primary energy savings compared to the state-of-the-art of biogas upgrading processes in the range of 50–75%. In the base case, methane loss is comparably high (2.7%) but can be reduced by approximately 75% by using [BDiMIM][TCM] as RTIL and by increasing the mass fraction of CFIL from 10 wt% to 20 wt%.

The expected savings in OPEX can be applied for the additional investment of the ionic liquid solvents which are more expensive than conventional solvents. Assuming an IL price at 65 EUR/kg, which is expected to be realistic when non-fluorinated substances were produced in large quantities, decent payback periods in the range of less than 5 years are calculated.

6. Perspectives

At present, the process is examined in a fully automated lab scale mini plant at DVGW Research Center at KIT, allowing continuous operation of an absorption/desorption cycle. In the near future the mini plant will be transferred to a biogas injection plant site, where it will be operated in parallel to the existing upgrading plant for long term stability measurements with real biogas feed.

Although it seems obvious from the present results achieved in the autoclave and the mini-plant that the regeneration of the solvent is possible in the desired temperature range, experimental investigations on this issue are still pending. There is a certain risk that the regeneration of the solvent might become a bottleneck in the process, as CO_2 desorption might be slow because it has to be physically transported from the bulk liquid to the phase boundary. Nevertheless, first tests are promising as supersaturation of physically dissolved CO_2 occurs in the liquid phase once the pressure is reduced. Supersaturation of CO_2 leads to spontaneous bubble formation in the liquid phase, resulting in an intensification of mass transfer which has a positive impact on overall regeneration performance.

Acknowledgements

The authors are thankful for the funding from MWK (Ministry of Science, Research and Arts) Baden-Wuerttemberg: 7533-10-5-105, the BMWi (Federal Ministry of Economic Affairs and Energy) and the DVGW (German Technical and Scientific Association for Gas and Water): 03KB104A-C.

References

[1] T. Welton, Room-temperature ionic liquids. Solvents for synthesis and catalysis, Chem. Rev. 99 (8) (1999) 2071–2084.
[2] P. Wasserscheid, T. Welton, Ionic Liquids in Synthesis, second ed., Wiley-VCH, Weinheim, 2008.
[3] R.D. Rogers, K.R. Seddon (Eds.), Ionic Liquids, American Chemical Society, Washington, DC, 2002.
[4] F. Heym, Dampfdruck und thermische Zersetzung reiner und geträgerter ionischer Flüssigkeiten, Dissertation, Bayreuth, 2013.
[5] M. Ramdin, Theo W. de Loos, T.J.H. Vlugt, State-of-the-art of CO_2 capture with ionic liquids, Ind. Eng. Chem. Res. 51 (24) (2012) 8149–8177.
[6] International Energy Agency, World Energy Outlook, 2015.
[7] H. Hiller, R. Reimert, F. Marschner, H.-J. Renner, W. Boll, E. Supp, M. Brejc, W. Liebner, G. Schaub, G. Hochgesand, C. Higman, P. Kalteier, W.-D. Müller, M. Kriebel, H. Schlichting, H. Tanz, H.-M. Stönner, H. Klein, W. Hilsebein, V. Gronemann, U. Zwiefelhofer, J. Albrecht, C.J. Cowper, H.E. Driesen, Gas Production, in: Ullmann's Encyclopedia of Industrial Chemistry, Wiley-VCH Verlag GmbH & Co. KGaA, Weinheim, Germany, 2000.
[8] A.L. Kohl, R. Nielsen, Gas Purification, fifth ed., Gulf Pub., Houston, Texas, 1997.
[9] M. Götz, J. Lefebvre, F. Mörs, A. McDaniel Koch, F. Graf, S. Bajohr, R. Reimert, T. Kolb, Renewable power-to-gas: a technological and economic review, Renew. Energy 85 (2016) 1371–1390.
[10] F. Graf, S. Bajohr (Eds.), Biogas: Erzeugung - Aufbereitung - Einspeisung, second ed., Oldenbourg Industrieverlag, München, 2013.
[11] A. Wellinger, J. Murphy, D. Baxter, The Biogas Handbook: Science, Production and Applications.
[12] S. Rönsch, J. Schneider, S. Matthischke, M. Schlüter, M. Götz, J. Lefebvre, P. Prabhakaran, S. Bajohr, Review on methanation – from fundamentals to current projects, Fuel 166 (2016) 276–296.
[13] DVGW Deutscher Verein des Gas- und Wasserfaches e. V., G 260 - Gasbeschaffenheit, 2013.
[14] DVGW Deutscher Verein des Gas- und Wasserfaches e. V., G 262 - Nutzung von Gasen aus regenerativen Quellen in der öffentlichen Gasversorgung.
[15] Deutsche Norm DIN 51624, Kraftstoffe für Kraftfahrzeuge - Erdgas Anforderungen und Prüfverfahren, 2008th ed.
[16] D. Stolten, V. Scherer, Process Engineering for CCS Power Plants, Wiley-VCH, Weinheim, 2011.
[17] BNetzA, Biogas-Monitoringbericht 2014: Bericht der Bundesnetzagentur über die Auswirkungen der Sonderregelungen für die Einspeisung von Biogas in das Erdgasnetz, 2014.
[18] IEA Bioenergy Task 40 und Task 37, Biomethane: Status and Factors Affecting Market Development and Trade, 2014.
[19] D. Deublein, A. Steinhauser, Biogas from Waste and Renewable Resources: An Introduction, second ed., Wiley-VCH Verlag, Weinheim, 2012.
[20] FNR e.V., Verteilung der Verfahren zur Biogasaufbereitung in Deutschland, available at < http://www.fnr.de/basisdaten/bioenergie/biogas.html > (accessed on July 15, 2016).
[21] M. Gupta, Eirik F. da Silva, A. Hartono, H.F. Svendsen, Theoretical study of differential enthalpy of absorption of CO_2 with MEA and MDEA as a function of temperature, J. Phys. Chem. B 117 (32) (2013) 9457–9468.
[22] Y.-Y. Jiang, G.-N. Wang, Z. Zhou, Y.-T. Wu, J. Geng, Z.-B. Zhang, Tetraalkylammonium amino acids as functionalized ionic liquids of low viscosity, Chem. Commun. (Cambridge, England) 2 (4) (2008) 505–507.
[23] H. Yu, Y.-T. Wu, Y.-Y. Jiang, Z. Zhou, Z.-B. Zhang, Low viscosity amino acid ionic liquids with asymmetric tetraalkylammonium cations for fast absorption of CO_2, New J. Chem. 33 (12) (2009) 2385.
[24] Mohd Basyaruddin Abdul Rahman, K. Jumbri, M. Basri, E. Abdulmalek, K. Sirat, A.B. Salleh, Synthesis and physico-chemical properties of new tetraethylammonium-based amino acid chiral ionic liquids, Molecules (Basel, Switzerland) 15 (4) (2010) 2388–2397.
[25] P. Navarro, M. Larriba, J. García, F. Rodríguez, Thermal stability and specific heats of [emim][DCA] + [emim][TCM] mixed ionic liquids, Thermochim. Acta 588 (2014) 22–27.
[26] M. Larriba, P. Navarro, J. García, F. Rodríguez, Separation of toluene from n-heptane, 2,3-dimethylpentane, and cyclohexane using binary mixtures of [4empy][Tf2N] and [emim][DCA] ionic liquids as extraction solvents, Sep. Purif. Technol. 120 (2013) 392–401.
[27] P. Scovazzo, D. Camper, J. Kieft, J. Poshusta, C. Koval, R. Noble, Regular solution theory and CO_2 gas solubility in room-temperature ionic liquids, Ind. Eng. Chem. Res. 43 (21) (2004) 6855–6860.
[28] D. Camper, J. Bara, C. Koval, R. Noble, Bulk-fluid solubility and membrane feasibility of Rmim-based room-temperature ionic liquids, Ind. Eng. Chem. Res. 45 (18) (2006) 6279–6283.
[29] Alistair W.T. King, A. Parviainen, P. Karhunen, J. Matikainen, Lauri K. Hauru, H. Sixta, I. Kilpelainen, Relative and inherent reactivities of imidazolium-based ionic liquids: the implications for lignocellulose processing applications, RSC Adv. 2 (21) (2012) 8020–8026.
[30] H. Rodríguez, J.F. Brennecke, Temperature and composition dependence of the density and viscosity of binary mixtures of water + ionic liquid, J. Chem. Eng. Data 51 (6) (2006) 2145–2155.
[31] J.G. Huddleston, A.E. Visser, W. Reichert, H.D. Matthew, G.A. Willauer, R.D. Rogers Broker, Characterization and comparison of hydrophilic and hydrophobic room temperature ionic liquids incorporating the imidazolium cation, Green Chem. 3 (4) (2001) 156–164.
[32] J. Jacquemin, P. Husson, A.A.H. Padua, V. Majer, Density and viscosity of several pure and water-saturated ionic liquids, Green Chem. 8 (2) (2006) 172–180.
[33] J. Jacquemin, P. Husson, V. Majer, Margarida F. Costa Gomes, Influence of the cation on the solubility of CO_2 and H_2 in ionic liquids based on the bis(trifluoromethylsulfonyl)imide anion, J. Sol. Chem. 36 (8) (2007) 967–979.
[34] A. Finotello, J.E. Bara, D. Camper, R.D. Noble, Room-temperature ionic liquids: temperature dependence of gas solubility selectivity, Ind. Eng. Chem. Res. 47 (10) (2008) 3453–3459.
[35] Z. Fang, Richard L. Smith, X. Qi, Production of Biofuels and Chemicals with Ionic Liquids, Springer, Dordrecht, Netherlands, 2014.

[36] A. Carlos, E. Nieto de Castro, A.L. Morais Langa, Manuel L. Matos, M.J.V. Lopes, F.J.V. Lourenço, M Soledade Santos, C.S. Lopes Santos, José N. Canongia, H.I.M. Veiga, M. Macatrão, J.M.S.S. Esperança, C.S. Marques, L.P.N. Rebelo, C.A.M. Afonso, Studies on the density, heat capacity, surface tension and infinite dilution diffusion with the ionic liquids [C4mim][NTf2], [C4mim][dca], [C2mim][EtOSO3] and [Aliquat][dca], Fluid Phase Equilibr. 294 (1–2) (2010) 157–179.
[37] L.G. Sánchez, J.R. Espel, F. Onink, G. Wytze Meindersma, André B. de Haan, Density, viscosity, and surface tension of synthesis grade imidazolium, pyridinium, and pyrrolidinium based room temperature ionic liquids, J. Chem. Eng. Data 54 (10) (2009) 2803–2812.
[38] L.M. Galán Sánchez, Functionalized Ionic Liquids: Absorption Solvents for Carbon Dioxide and Olefin Separation, Dissertation, Eindhoven, 2008.
[39] L.F. Zubeir, G.E. Romanos, Wilko M.A. Weggemans, B. Iliev, Thomas J.S. Schubert, M.C. Kroon, Solubility and diffusivity of CO_2 in the ionic liquid 1-butyl-3-methylimidazolium tricyanomethanide within a large pressure range (0.01 MPa to 10 MPa), J. Chem. Eng. Data 60 (6) (2015) 1544–1562.
[40] P. Bonhôte, A.-P. Dias, N. Papageorgiou, K. Kalyanasundaram, M. Grätzel, Hydrophobic, highly conductive ambient-temperature molten salts, Inorg. Chem. 35 (5) (1996) 1168–1178.
[41] X.L. Papatryfon, N.S. Heliopoulos, I.S. Molchan, L.F. Zubeir, N.D. Bezemer, M.K. Arfanis, A.G. Kontos, V. Likodimos, B. Iliev, G.E. Romanos, P. Falaras, K. Stamatakis, K.G. Beltsios, M.C. Kroon, G.E. Thompson, J. Klöckner, Thomas J.S. Schubert, CO_2 capture efficiency, corrosion properties, and ecotoxicity evaluation of amine solutions involving newly synthesized ionic liquids, Ind. Eng. Chem. Res. 53 (30) (2014) 12083–12102.
[42] Solvionic, Product information, available at < http://en.solvionic.com/files/solvionic/fiches/Product_Im0405b_R1.pdf > .
[43] O.O. Okoturo, T.J. VanderNoot, Temperature dependence of viscosity for room temperature ionic liquids, J. Electroanal. Chem. 568 (2004) 167–181.
[44] A.N. Soriano, B.T. Doma, M.-H. Li, Carbon dioxide solubility in some ionic liquids at moderate pressures, J. Taiwan Inst. Chem. Eng. 40 (4) (2009) 387–393.
[45] K.R. Harris, M. Kanakubo, L.A. Woolf, Temperature and pressure dependence of the viscosity of the ionic liquids 1-hexyl-3-methylimidazolium hexafluorophosphate and 1-butyl-3-methylimidazolium bis(trifluoromethylsulfonyl)imide, J. Chem. Eng. Data 52 (3) (2007) 1080–1085.
[46] Y. Hou, R.E. Baltus, Experimental measurement of the solubility and diffusivity of CO_2 in room-temperature ionic liquids using a transient thin-liquid-film method, Ind. Eng. Chem. Res. 46 (24) (2007) 8166–8175.
[47] S.D. Chambreau, A.C. Schenk, A.J. Sheppard, G.R. Yandek, G.L. Vaghjiani, J. Maciejewski, C.J. Koh, A. Golan, S.R. Leone, Thermal decomposition mechanisms of alkylimidazolium ionic liquids with cyano-functionalized anions, J. Phys. Chem. A 118 (47) (2014) 11119–11132.
[48] Y. Zhang, P. Yu, Y. Luo, Absorption of CO_2 by amino acid-functionalized and traditional dicationic ionic liquids: properties, Henry's law constants and mechanisms, Chem. Eng. J. 214 (2013) 355–363.
[49] Y.C. Lien, W.W. Nawar, Thermal decomposition of some amino acids. Valine, leucine and lsoleucine, J. Food Sci. 39 (5) (1974) 911–913.
[50] A. Seeberger, A.-K. Andresen, A. Jess, Prediction of long-term stability of ionic liquids at elevated temperatures by means of non-isothermal thermogravimetrical analysis, PCCP 11 (41) (2009) 9375–9381.
[51] F. Ortloff, J. Bohnau, F. Graf, T. Kolb, Removal of oxygen from (bio-)methane via catalytic oxidation of CH_4—reaction kinetics for very low O_2:CH_4 ratios, Appl. Catal. B 182 (2016) 375–384.
[52] F. Ortloff, J. Bohnau, U. Kramar, F. Graf, T. Kolb, Studies on the influence of H_2S and SO_2 on the activity of a PdO/Al_2O_3 catalyst for removal of oxygen by total oxidation of (bio-)methane at very low O_2:CH_4 ratios, Appl. Catal. B 182 (2016) 550–561.
[53] J.J. Carroll, J.D. Slupsky, A.E. Mather, The solubility of carbon dioxide in water at low pressure, J. Phys. Chem. Ref. Data 20 (6) (1991) 1201–1209.
[54] D.R. Lide, CRC Handbook of Chemistry and Physics: A Ready-reference Book of Chemical and Physical Data, 89th ed., CRC, Boca Raton, Fla., London, 2008.
[55] M. Götz, F. Ortloff, R. Reimert, O. Basha, B.I. Morsi, T. Kolb, Evaluation of organic and ionic liquids for three-phase methanation and biogas purification processes, Energy Fuels 27 (8) (2013) 4705–4716.
[56] A.V. Rayer, A. Henni, P. Tontiwachwuthikul, High pressure physical solubility of carbon dioxide (CO_2) in mixed polyethylene glycol dimethyl ethers (Genosorb 1753), Can. J. Chem. Eng. 90 (3) (2012) 576–583.
[57] D. Kerle, Untersuchung der Löslichkeit von Gasen in ionischen Flüssigkeiten mit Methoden der molekulardynamischen Simulation. Dissertation, Rostock, 2013.
[58] S. Bishnoi, G.T. Rochelle, Absorption of carbon dioxide into aqueous piperazine: reaction kinetics, mass transfer and solubility, Chem. Eng. Sci. 55 (22) (2000) 5531–5543.
[59] S.S. Laddha, J.M. Diaz, P.V. Danckwerts, The N_2O analogy: the solubilities of CO_2 and N_2O in aqueous solutions of organic compounds, Chem. Eng. Sci. 36 (1) (1981) 228–229.
[60] L. Kucka, J. Richter, E.Y. Kenig, A. Górak, Determination of gas–liquid reaction kinetics with a stirred cell reactor, Sep. Purif. Technol. 31 (2) (2003) 163–175.
[61] S. Ali, Kinetic study of the reaction of diethanolamine with carbon dioxide in aqueous and mixed solvent systems—application to acid gas cleaning, Sep. Purif. Technol. 38 (3) (2004) 281–296.
[62] F. Pani, A. Gaunand, R. Cadours, C. Bouallou, D. Richon, Kinetics of absorption of CO_2 in concentrated aqueous methyldiethanolamine solutions in the range 296 K to 343 K, J. Chem. Eng. Data 42 (2) (1997) 353–359.
[63] X. Zhang, C.-F. Zhang, S.-J. Qin, Z.-S. Zheng, A kinetics study on the absorption of carbon dioxide into a mixed aqueous solution of methyldiethanolamine and piperazine, Ind. Eng. Chem. Res. 40 (17) (2001) 3785–3791.
[64] Y.E. Kim, J.A. Lim, S.K. Jeong, Y.I. Yoon, S.T. Bae, S.C. Nam, Comparison of carbon dioxide absorption in aqueous MEA DEA, TEA, and AMP solutions, Bull. Korean Chem. Soc. 34 (3) (2013) 783–787.
[65] S. Bishnoi, G.T. Rochelle, Thermodynamics of piperazine/methyldiethanolamine/water/carbon dioxide, Ind. Eng. Chem. Res. 41 (3) (2002) 604–612.
[66] H. Svensson, C. Hulteberg, H.T. Karlsson, Heat of absorption of CO_2 in aqueous solutions of N-methyldiethanolamine and piperazine, Int. J. Greenhouse Gas Control 17 (2013) 89–98.
[67] BMWi, Energie in Deutschland: Trends und Hintergründe zur Energieversorgung, 2013.
[68] R.D. Rogers, K.R. Seddon, S. Volkov, Green Industrial Applications of Ionic Liquids, Springer, Netherlands, Dordrecht, 2002.